Scuola di Dottorato in Ingegneria Leonardo da Vinci – a.a. 2009/10

PROPRIETÀ MECCANICHE, OTTICHE, ELETTRONICHE DEI MATERIALI ALLE PICCOLE E PICCOLISSIME SCALE

Versione 1 – Ottobre 2010 – http://www.df.unipi.it/~fuso/dida

Parte 6

Proprietà speciali di strutture nanodimensionate: l'esempio dei nanotubi di carbonio; dalla piccolissima alla piccola scala

Me 6.10 13-16 aula S1 DF

Outlook

- Mechanical properties of individual nanostructures may often reveal unexpected features such as: huge Young modulus, enhanced stiffness and strength upon perturbations

- CNTs are an excellent example:
  - CNT structure;
  - CNT fabrication;
  - CNT electronic properties (a few words);
  - Some attempts to interpret the CNT mechanical properties
  - How to use CNTs and how to produce nanocomposites

- A different topic, worth to be briefly mentioned: the relationships and interplay between small and ultra-small in localized stress applications (simulations and considerations)

Carbon NanoTubes (CNT)

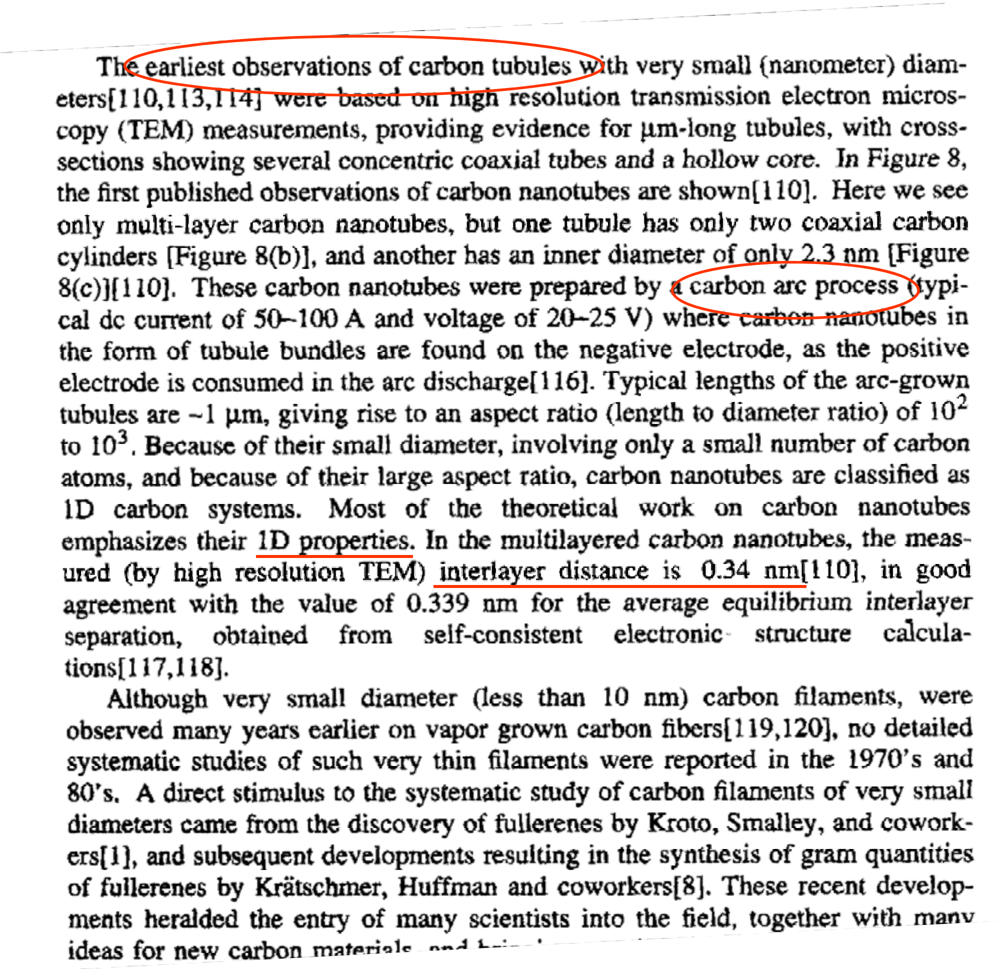

The earliest observations of carbon tubules with very small (nanometer) diameters[110,113,114] were based on high resolution transmission electron microscopy (TEM) measurements, providing evidence for µm-long tubules, with cross-sections showing several concentric coaxial tubes and a hollow core. In Figure 8, the first published observations of carbon nanotubes are shown[110]. Here we see only multi-layer carbon nanotubes, but one tubule has only two coaxial carbon cylinders [Figure 8(b)], and another has an inner diameter of only 2.3 nm [Figure 8(c)][110]. These carbon nanotubes were prepared by a carbon arc process (typical dc current of 50–100 A and voltage of 20–25 V) where carbon nanotubes in the form of tubule bundles are found on the negative electrode, as the positive electrode is consumed in the arc discharge[116]. Typical lengths of the arc-grown tubules are ~1 µm, giving rise to an aspect ratio (length to diameter ratio) of 10^2 to 10^3. Because of their small diameter, involving only a small number of carbon atoms, and because of their large aspect ratio, carbon nanotubes are classified as 1D carbon systems. Most of the theoretical work on carbon nanotubes emphasizes their 1D properties. In the multilayered carbon nanotubes, the measured (by high resolution TEM) interlayer distance is 0.34 nm[110], in good agreement with the value of 0.339 nm for the average equilibrium interlayer separation, obtained from self-consistent electronic structure calculations[117,118].

Although very small diameter (less than 10 nm) carbon filaments, were observed many years earlier on vapor grown carbon fibers[119,120], no detailed systematic studies of such very thin filaments were reported in the 1970's and 80's. A direct stimulus to the systematic study of carbon filaments of very small diameters came from the discovery of fullerenes by Kroto, Smalley, and coworkers[1], and subsequent developments resulting in the synthesis of gram quantities of fullerenes by Krätschmer, Huffman and coworkers[8]. These recent developments heralded the entry of many scientists into the field, together with many ideas for new carbon materials

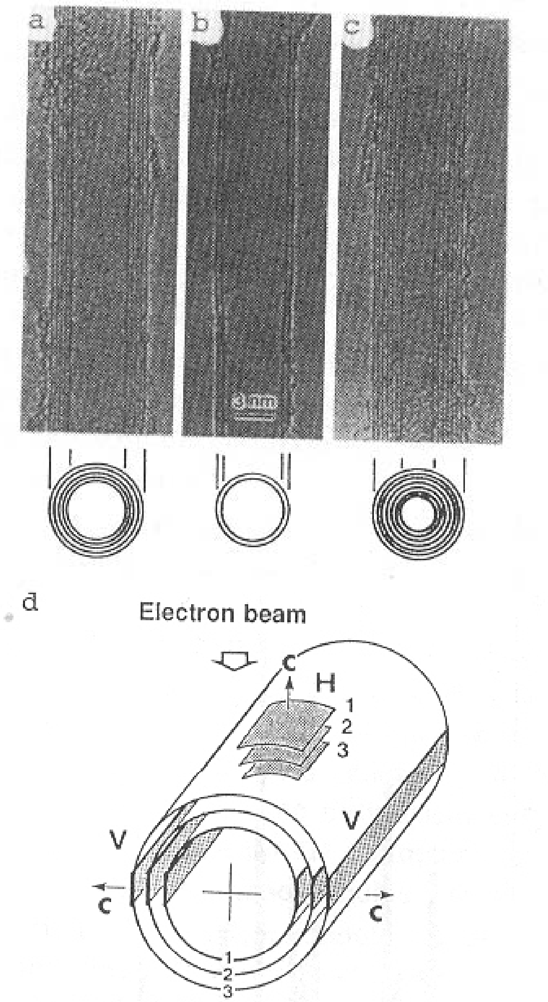

FIGURE 8. The observation of N concentric carbon tubules with various inner diameters d_i and outer diameters d_o reported by Iijima using TEM. (a) $N = 5$, $d_o = 6.7$ nm, (b) $N = 2$, $d_o = 5.5$ nm, and (c) $N = 7$, $d_i = 2.3$ nm, $d_o = 6.5$ nm. Each cylinder is described by its diameter and chiral angle. The sketch (d) indicates how the interference pattern for the parallel planes labeled H are used to determine the chiral angle θ, which is the angle between the tubule axis and the nearest zigzag axis defined in Figure 10[110].

Work on fullerenes produced a revival of interest for (already known) ***filamentary carbon nanostructures (nanotubes)***

From graphite to CNT

Highly Oriented Pyrolithic Graphite (HOPG) surface

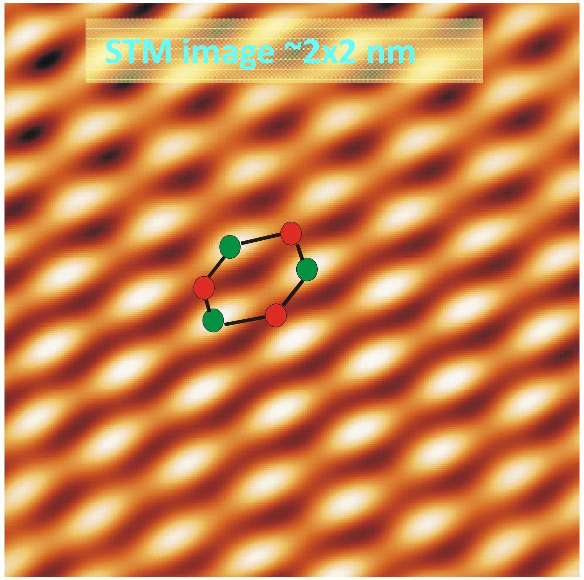

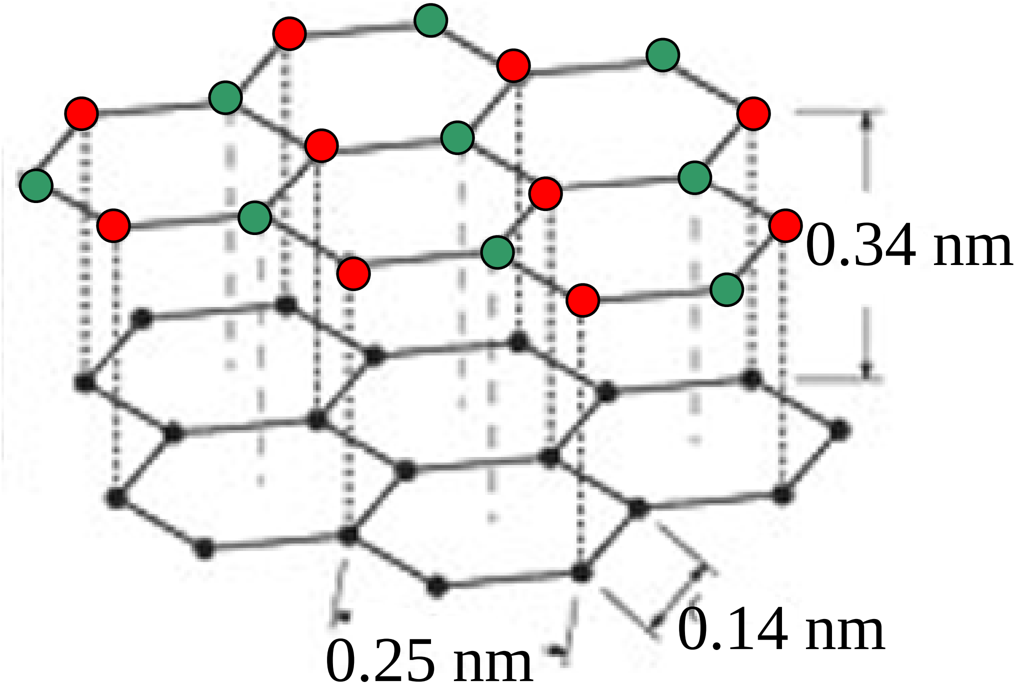

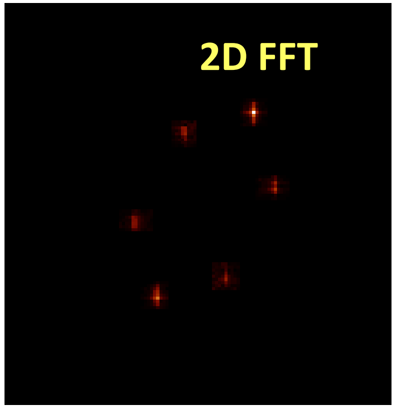

Two different positions of the carbon atoms in the graphite crystal lattice are possible: one with a neighbouring atom in the plane below (red) and one without a neighbour in the lattice below (green).
Consequently the electrical conductivity of the graphite surface varies locally slightly (different electronic density of states) so that the atoms without neighbours appear "higher" than the others (see e.g. I.P. Batra et al. Surf Sci 181 (1987) 126). This also causes the lattice constant between the bright ‘hills’ to have the higher value of 0.25nm than the nearest neighbour distance in the graphite lattice of 0.14nm.

Single and multiwall CNT

CNT: a graphite plane (graphene) is wounded in a cylindrical shape

SWNT: single nanotube
MWNT: concentric nanotubes with different diameters

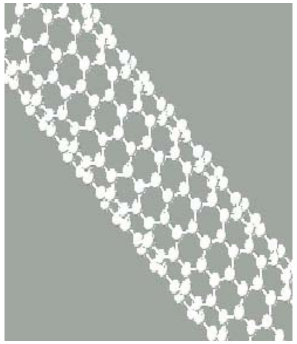

Single Wall NT

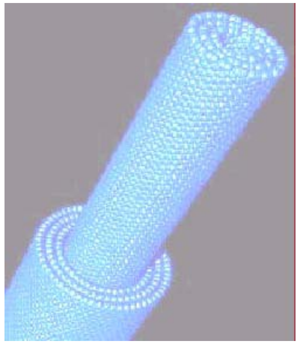

Multiple Wall N

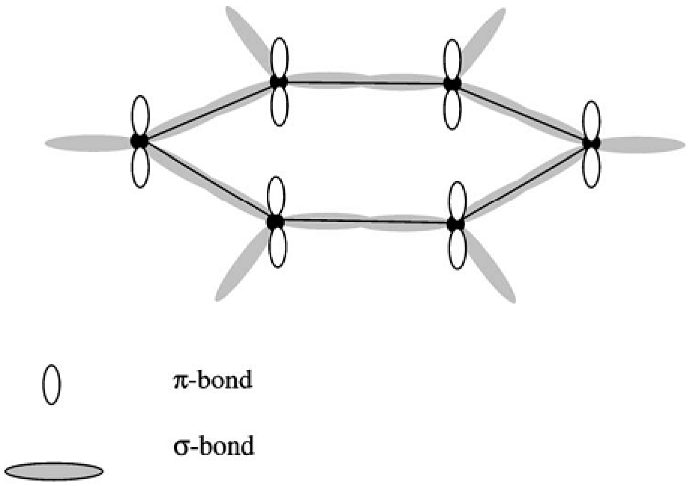

Strong σ (sp^2) bonds responsible for "in-plane" (i.e., in-surface) structure

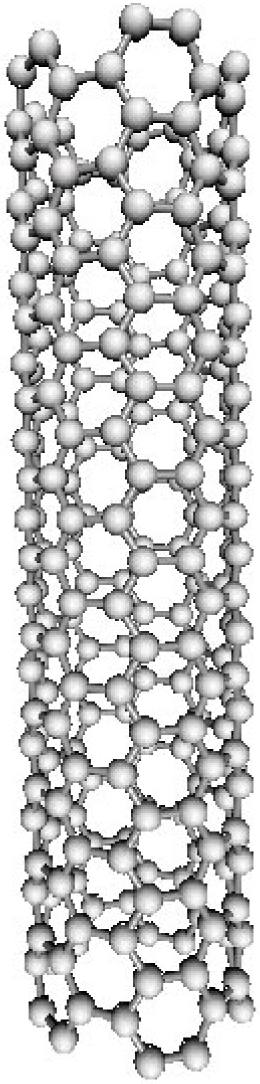

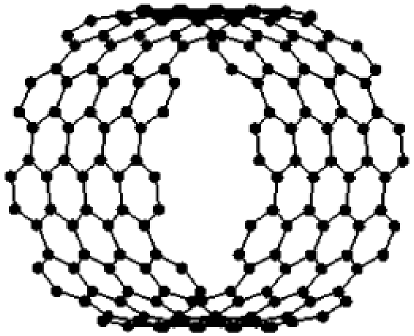

Fig. 1. Molecular structure of a section of (10, 10) CNT. Each node shown is a carbon atom and lines are the chemical bonds.

Materiale sui CNT tratto in parte da un seminario di Andrea Ferrari, EDM - Cambridge University (lug. 2002)

CNT families

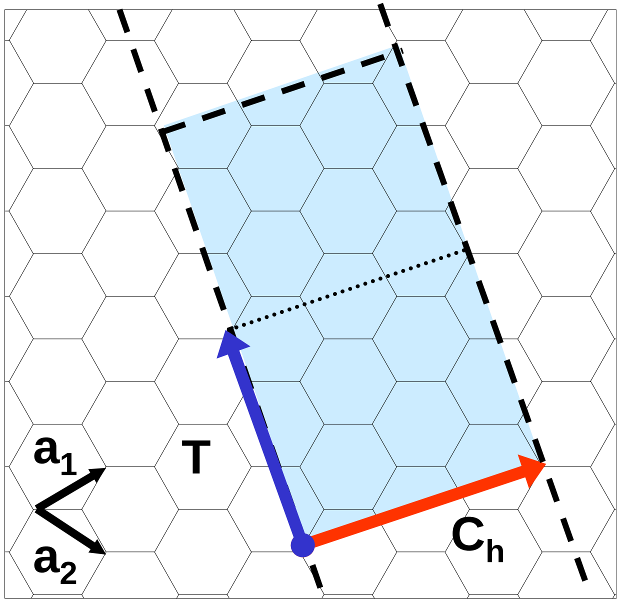

Regular structures with sp^2 bonds

Unit cell described by:

- chiral vector

  $\mathbf{C_h} = n\mathbf{a_1} + m\mathbf{a_2} \equiv (n, m)\ \forall\ n,m \in Z$

- translation vector

  $\mathbf{T} = t_1\mathbf{a_1} + t_2\mathbf{a_2}\ \ \forall\ t_1, t_2 \in Z$

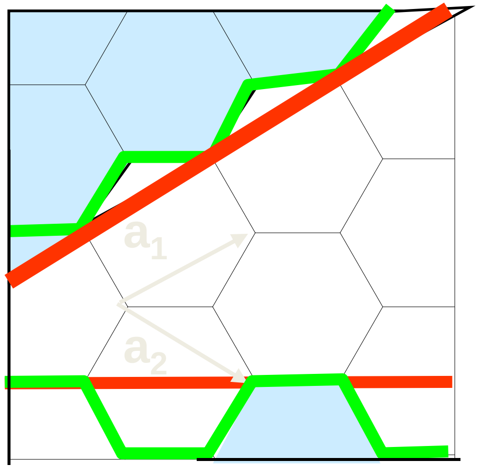

Zigzag (n, 0) tube
$\mathbf{C_h}$ // $\mathbf{a_1}$ (or $\mathbf{a_2}$)

CNT diameter: $d_{NT} \propto \sqrt{(m^2 + n^2 + nm)}$

Armchair (n, n) tube

[Chiral (n, m) tube]

CNT structure uniquely determined by (n, m)

First neighbor distance ~ 1.42 Å

CNT fabrication I

Nanotubes can be produced with many techniques
Typically, vapor phase is involved to produce nanotubes from carbon atoms
Typically, "violent" methods are required to induce strongly collisional conditions

Electric arc discharge (similar to fullerene production methods)

Laser ablation (similar to cluster production methods)

Plasma Ehnanced Chem Vap Dep (PE-CVD)

Chemical Vapor Deposition (CVD)

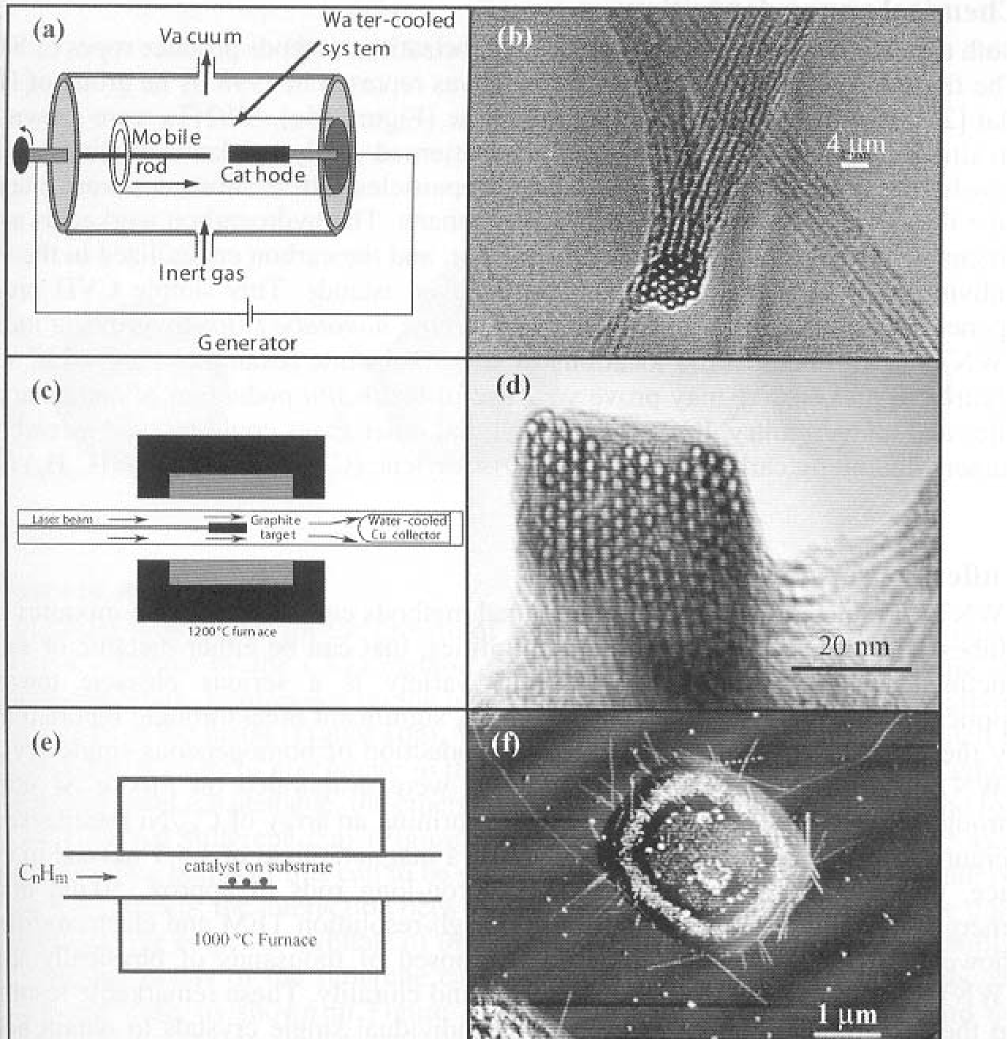

CNT fabrication II

Pulsed Laser Ablation → SWCNT with good diameter control
Arc discharge → large rates, low control (mostly MWCNT)
PE-CVD from C_xH_x → large rates, fair control

Laser Ablation

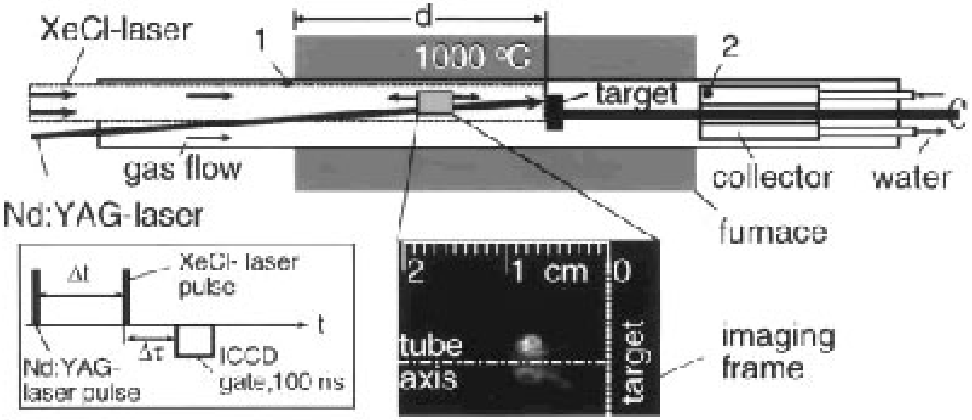

Fig. 1. Schematic of the 2″-diameter quartz tube and hot furnace used for laser vaporization growth of SWNT with in situ LIL-imaging and spectroscopy diagnostics. Beam geometries and imageable area are indicated. The *black dots* and the *numbers* show the collection points of the ablated material: 1-upstream; 2-collector. The C/Ni/Co target was positioned at two distances, *d*, from the front of the furnace. The *inset on the left* shows the relative timing between ablation (Nd:YAG) and and LIL-probe (XeCl) laser pulses (Δ*t*), and the ICCD gate delay after the XeCl laser, (Δτ)

See Puretzky, Geohegan,…
Appl. Phys. A 70 153 (2000)

PE-CVD

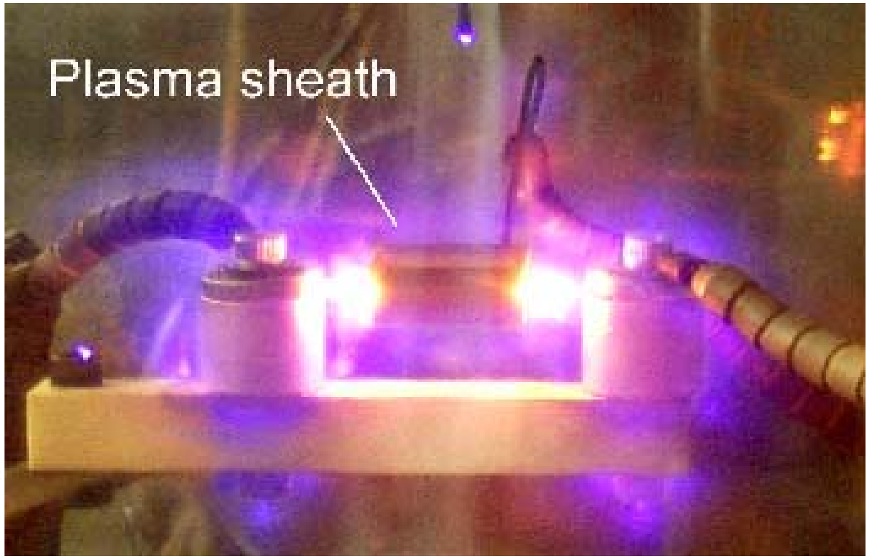

- Up to 900°C heated stage
- C_2H_2/NH_3 up to 200sccm

Role of catalyzers I

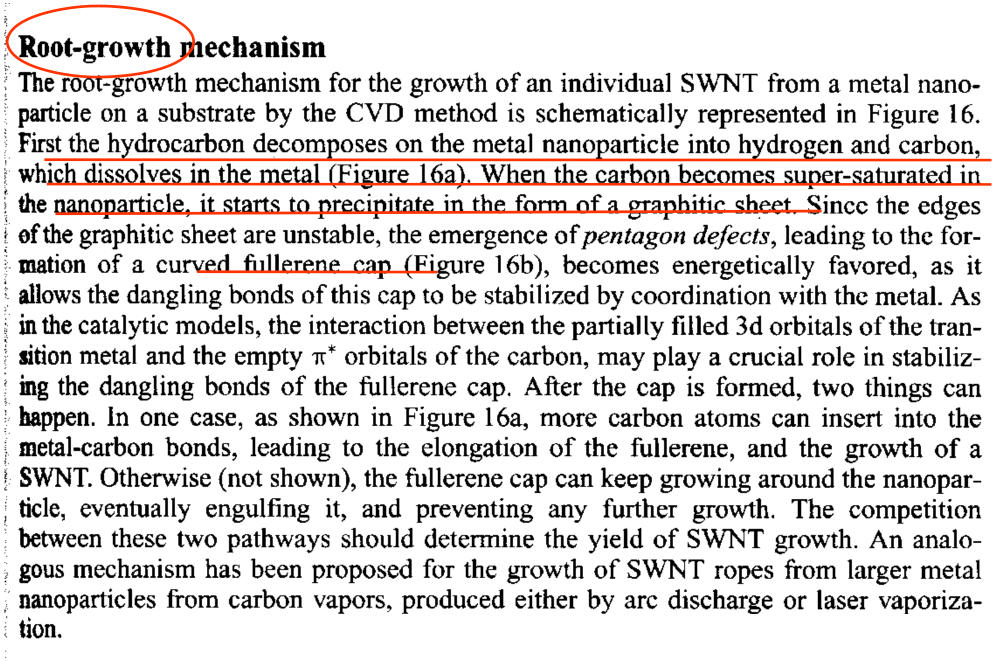

Root-growth mechanism

The root-growth mechanism for the growth of an individual SWNT from a metal nanoparticle on a substrate by the CVD method is schematically represented in Figure 16. First the hydrocarbon decomposes on the metal nanoparticle into hydrogen and carbon, which dissolves in the metal (Figure 16a). When the carbon becomes super-saturated in the nanoparticle, it starts to precipitate in the form of a graphitic sheet. Since the edges of the graphitic sheet are unstable, the emergence of *pentagon defects*, leading to the formation of a curved fullerene cap (Figure 16b), becomes energetically favored, as it allows the dangling bonds of this cap to be stabilized by coordination with the metal. As in the catalytic models, the interaction between the partially filled 3d orbitals of the transition metal and the empty π^* orbitals of the carbon, may play a crucial role in stabilizing the dangling bonds of the fullerene cap. After the cap is formed, two things can happen. In one case, as shown in Figure 16a, more carbon atoms can insert into the metal-carbon bonds, leading to the elongation of the fullerene, and the growth of a SWNT. Otherwise (not shown), the fullerene cap can keep growing around the nanoparticle, eventually engulfing it, and preventing any further growth. The competition between these two pathways should determine the yield of SWNT growth. An analogous mechanism has been proposed for the growth of SWNT ropes from larger metal nanoparticles from carbon vapors, produced either by arc discharge or laser vaporization.

Metal nanoparticles (typ Ni or Co) used to enhance and control nanotube formation

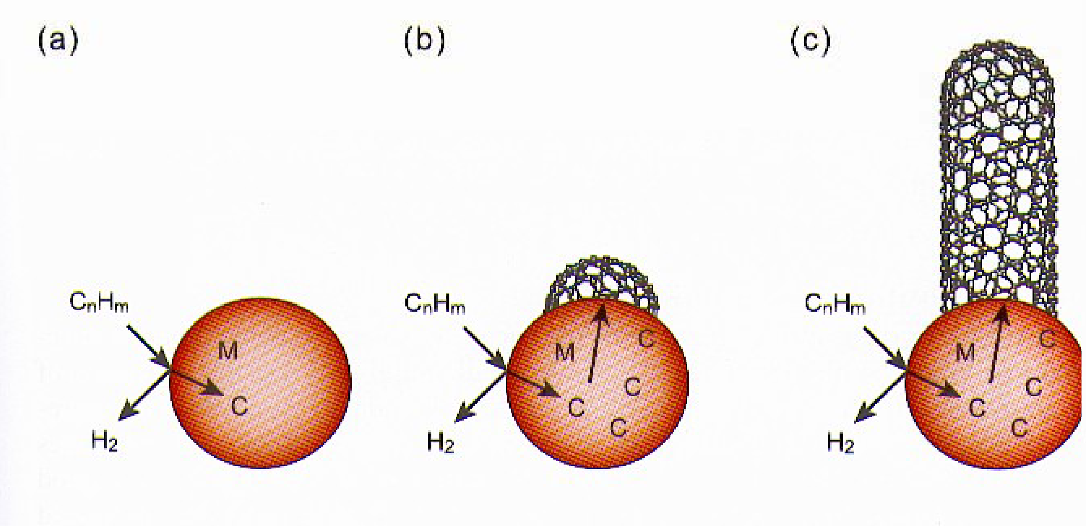

Figure 16: Root-growth mechanism for the formation of a single-wall carbon nanotube from a metal nanoparticle, by chemical vapor deposition:
(a) decomposition of the hydrocarbon on the nanoparticle and solubilization of the carbon therein.
(b) nucleation by formation of a fullerene cap.
(c) elongation of the SWNT by incorporation of further carbon into the metal-carbon bonds at the growing end.

Role of catalyzers II

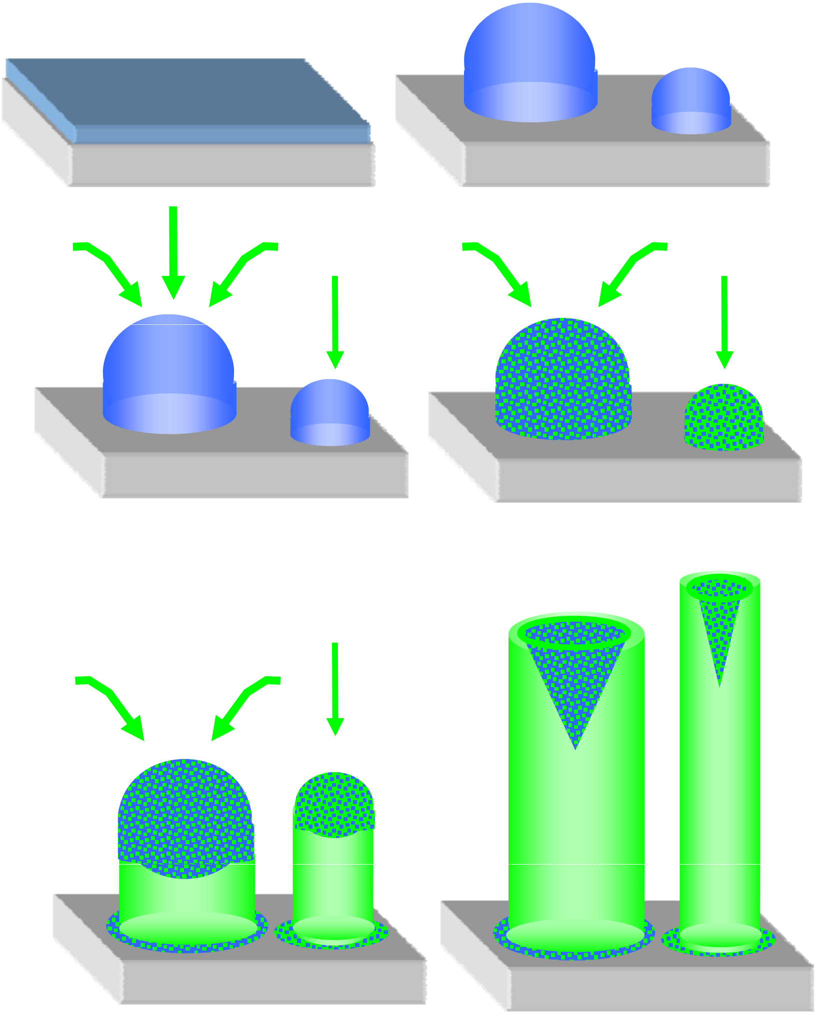

Alternative picture (Vapor Liquid Solid – VLS method)

- During annealing/etching the metal layer dewets the substrate forming droplets
- Carbon ***dissolves into*** the catalyst material and forms a solid solution
- ***After saturation***, carbon precipitates starting the NT growth
- The metal droplet is lifted at the growing edge

Role of catalyzers III

Metal nanoparticles can be "deposited" onto the substrate

⇓

If a nanoparticle pattern is structured onto the substrate, structured CNT growth can be achieved!!

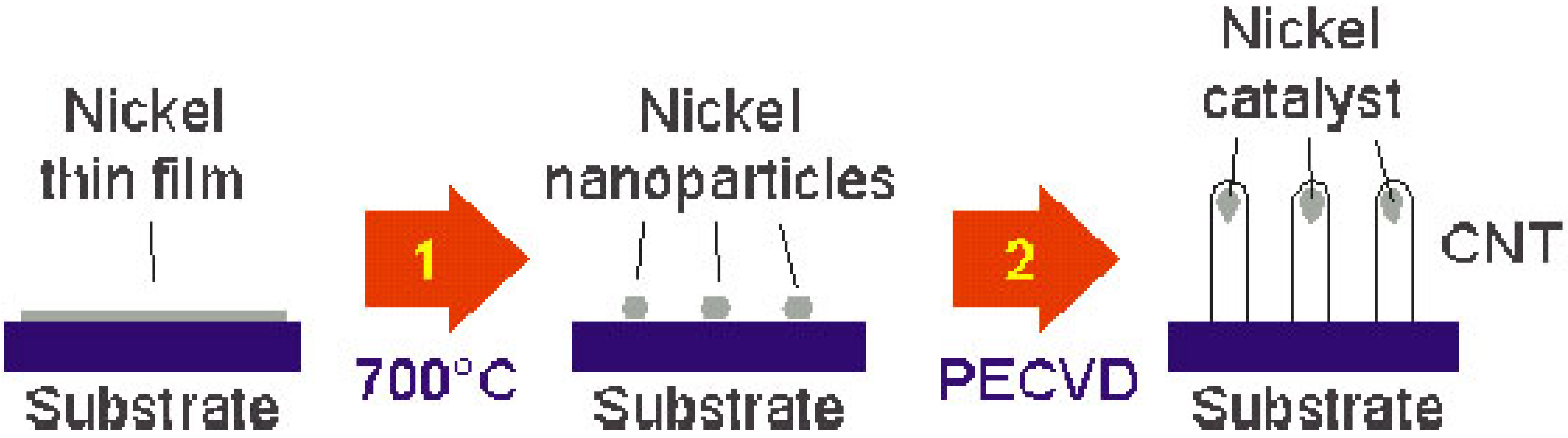

- **Step 1**: At 700°C (growth temp), Ni film sinters into catalyst nanoparticles.
- **Step 2**: PECVD - C_2H_2 is the growth gas for CNTs, NH_3 is the etching gas for unwanted a-C.

Role of catalyzers IV

Effect of nanoparticle size in CNT growth

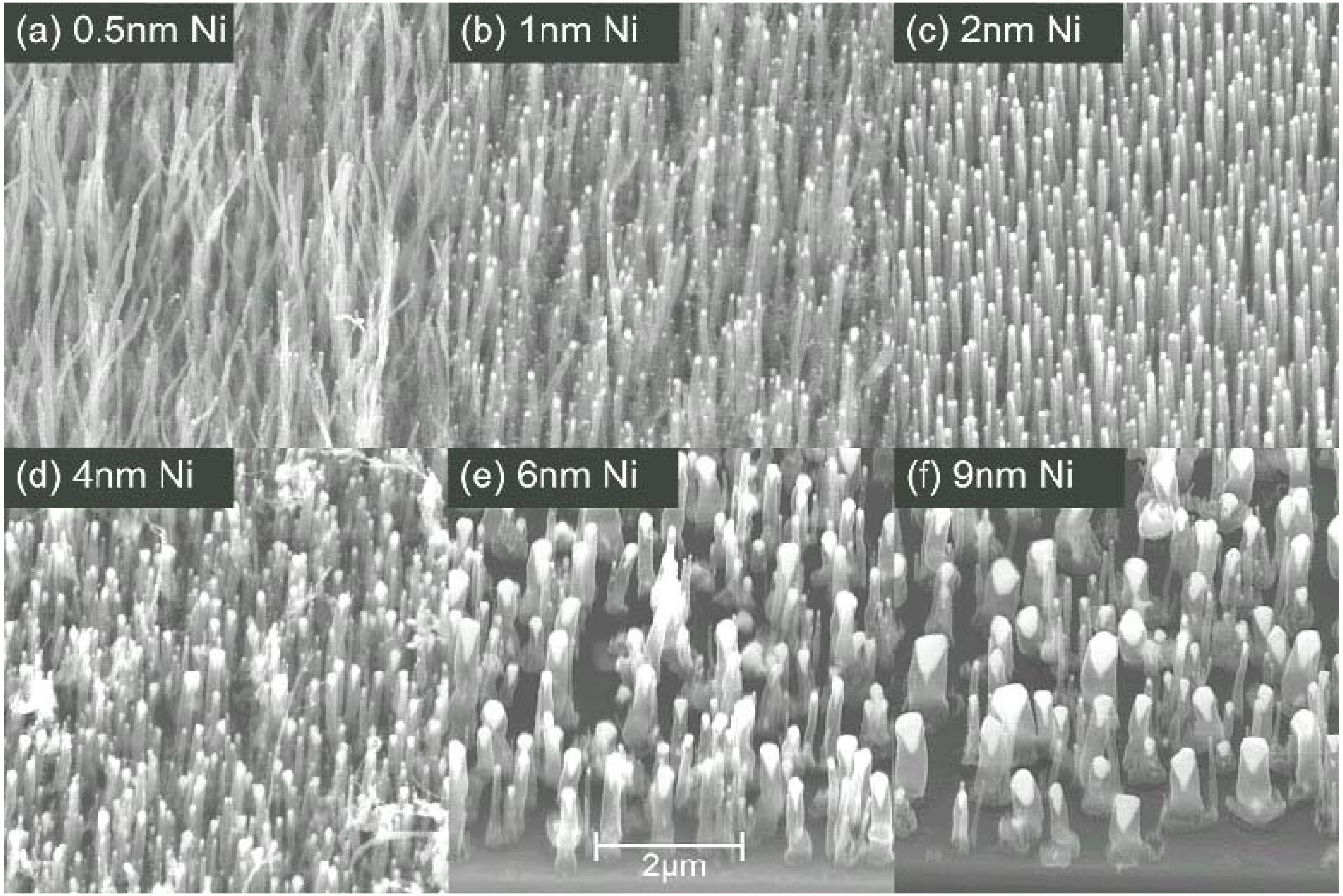

CNT patterns

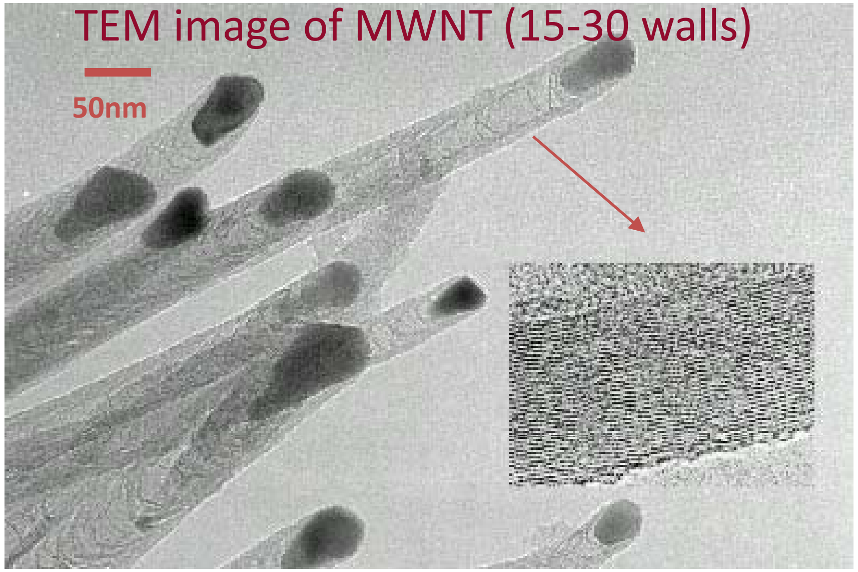

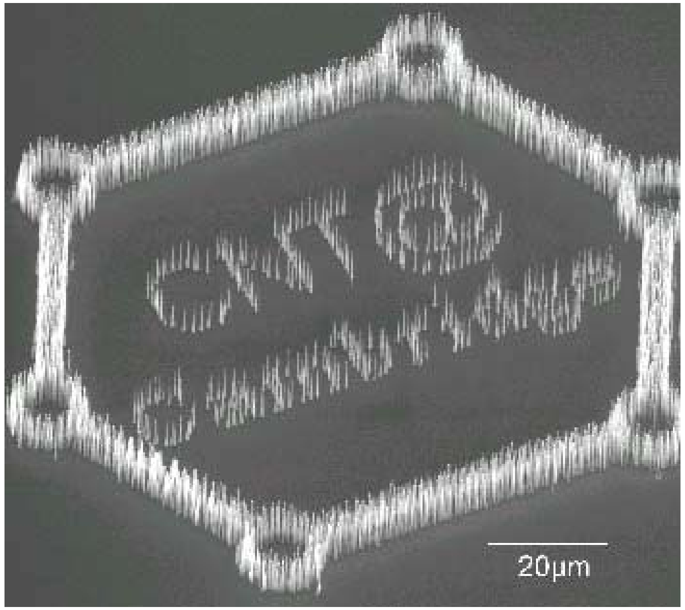

Nanoparticle patterns can be achieved by lithography leading to CNT patterns

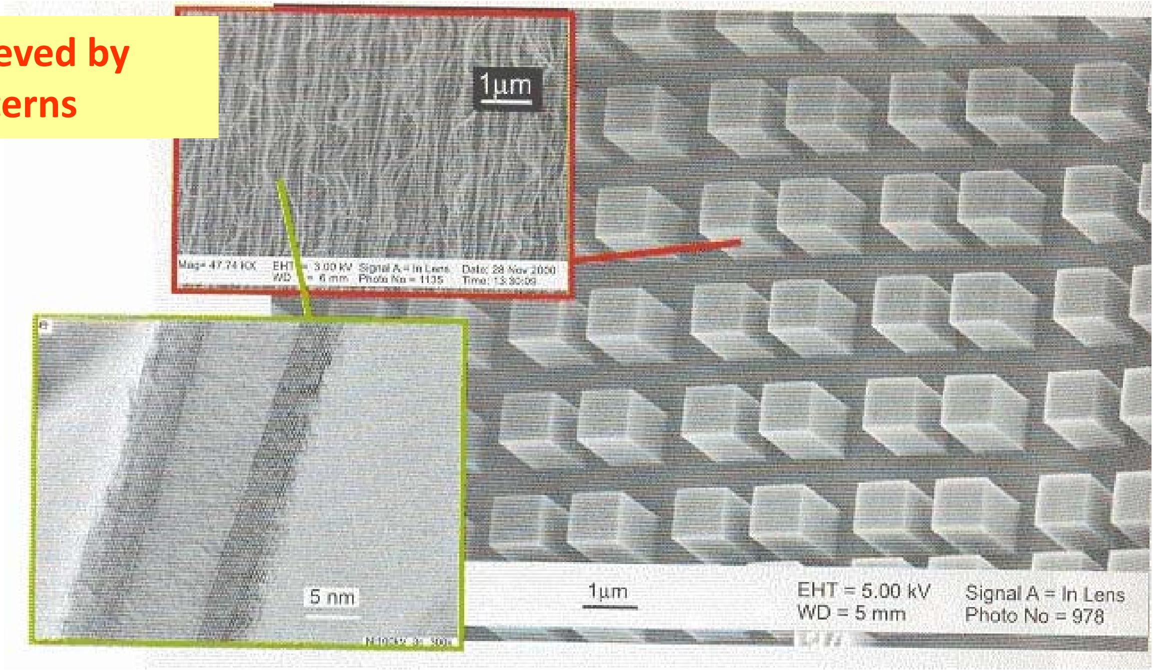

Figure 18: Nanotube blocks created by catalyst mediated growth. The tubes are generated from iron catalyst pads (100 × 100 µm) patterned by the lift-off technique. The first inset shows that each block consists of numerous nanotubes with a length exceeding 100 µm. The second inset shows a TEM-image of a single nanotube revealing that the tubes are multiwall with about 16 shells and a diameter of approximately 20 nm.

Electronic structure of CNT I

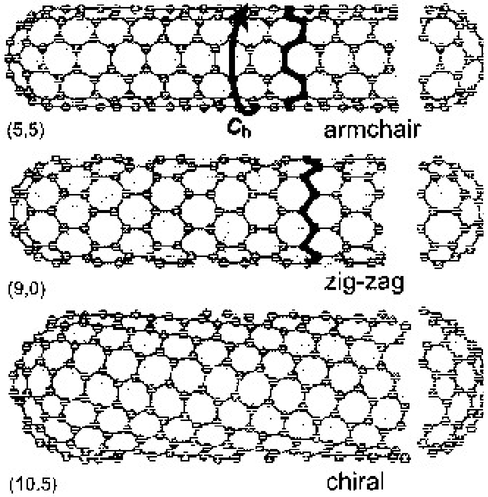

Figure 4: Examples of CNTs with different circumference vectors C_h [5].

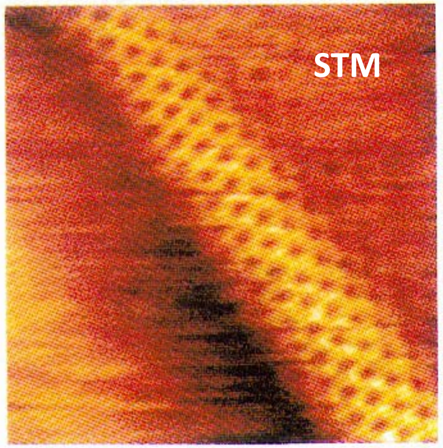

Figure 5: STM image at 77 K of a SWNT at the surface of a rope [6].

Da R. Waser Ed., Nanoelectronics and information technology (Wiley-VCH, 2003)

2.1 Geometrical Structure

The structure of CNTs is described by the circumference vector or **chiral vector C_h**, which represents the full circumference of the tube. It is defined by

$$C_h = n\boldsymbol{a}_1 + m\boldsymbol{a}_2 \tag{1}$$

where $\boldsymbol{a}_1$ and $\boldsymbol{a}_2$ are the unit vectors in the hexagonal lattice, and n and m are integers (Figure 1). C_h also defines the propagation vector $\boldsymbol{P}_h$ representing the periodicity of the tube parallel to the tube axis. Furthermore, it settles the so-called chiral angle which is the angle between C_h and a_1. If either n or m are zero, the chiral angle is 0° and the structure is called *zig-zag*. If $n = m$, the chiral angle is 30° and the structure is called *armchair* (Figure 4). All other nanotubes show chiral angles between 0° and 30°. They are known as *chiral* nanotubes because they produce a mirror image of their structure upon an exchange of n and m.

Experimentally, the diameter of nanotubes is frequently determined by TEM, STM or AFM. The chiral structure can be determined by STM (Figure 5).

2.2 Electronic Structure of Graphene

For the discussion of the electronic structure of CNTs, we start again with graphene. As an extension of the description of fused benzene (Chap. 5), in graphene, a bonding π-band and an anti-bonding π^*-band is formed from the overlap between $2p_z$-AOs of adjacent atoms. P. R. Wallace [7] derived an expression for the 2-D energy states, W_{2D}, of the π-electrons in the graphene plane as a function of the wave vectors k_x and k_y (see also [8]):

DOS

$$W_{2D}(k_x, k_y) = \pm\gamma_0 \left[1 + 4\cos\left(\frac{\sqrt{3}k_x a}{2}\right)\cos\left(\frac{k_y a}{2}\right) + 4\cos^2\left(\frac{k_y a}{2}\right)\right]^{1/2} \tag{2}$$

where γ_0 denotes the nearest-neighbour overlap (or: transfer) integral and $a = 0.246$ nm is the in-plane lattice constant. The two different signs in Eq. (2) represent the π- and π^*-band. The calculations show that the π- and π^*-band just touch each other at the corners of the 2-D Brillouin zone (Figure 6). In the vicinity of the Γ point, the dispersion relation is parabolically shaped, while towards the corners (K points) it shows a linear $W(k)$ dependence. At $T = 0$ K, the π-band is completely filled with electrons and the π^*-band is empty. Because the bands only touch at the K points, integration over the Fermi surface (which is a line for a two-dimensional system) results in a vanishing density of states. On the other hand no energy gap exists in the graphene dispersion relation. This means we are dealing with the unusual situation of a gapless semiconductor. (The real graphite yet is a metal since the bands overlap by approx. 40 meV due to the interaction of the graphene planes.)

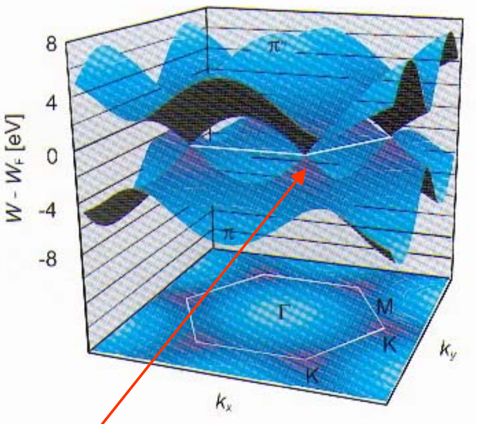

Figure 6: 3-D illustration of the dispersion relation of graphene.

Graphene: zero-gap semiconductor

Electronic structure of CNT II

2.3 Electronic Structure of Carbon Nanotubes

For the description of the band structure of graphene, it has been assumed that the graph ene plane is infinite in two dimensions. For CNTs, we have a structure which is macro scopic along the tube axis, but the circumference is in atomic dimensions. Hence, whi the density of allowed quantum mechanical states in axial direction will be high, t number of states in the circumferential direction will be very limited. More precisely, t roll-up by the chiral vector C_h leads to periodic boundary conditions in the circumfere tial direction. Quantum mechanically, these boundary conditions define allowed mod (1-D states) along the tube axis according to:

$$\boxed{C_h \cdot \boldsymbol{k} = 2\pi j} \quad \text{with} \quad |j| = 0, 1, 2, \ldots$$

In the case of arm-chair tubes, the periodic boundary condition yield allowed values t the wave vector in circumferential direction according to:

$$k_{y,j} = \frac{j}{q_y} \frac{2\pi}{\sqrt{3}a}$$

where $q_y = n = m$. For the armchair geometry, the tube axis is identical to the x-direction and the circumference represents the y-direction. As an example of an armchair tube, Figure 7 shows the dispersion relation, the projection of the allowed 1-D states onto the first Brillouin zone of graphene, as well as the $W(k_x)$ relation for a (3,3) tube. Due to the periodic boundary conditions, i. e. by inserting Eq. (4) into Eq. (2), the allowed states condense into lines (black lines in Figure 7a). Here, there are $q_y = 3$ lines on either side of the center of the Brillouin zone and an additional line going through the center. In case of a (3,3) tube the allowed states include the K points. Since the system is now one-dimensional in an electronic sense, different from the case of graphene, the integration over the Fermi surface (which is the sum over the Fermi points) yields a finite density of states at the Fermi energy. The (3,3) tube, and armchair tubes in general, show a *metallic*

Periodic boundary conditions in armchair CNT affect the DOS

Electronic configuration for armchair CNT indicates superposition of valence and conduction bands

Transport properties are that of a conductor (*metallic CNT*)

Figure 7: Dispersion relation of a (3,3) CNT.
(a) 3-D illustration of the dispersion relation for graphene including the allowed states for the (3,3) CNT. The periodic boundary conditions along the circumference of the tube result in a discrete set of allowed k_y values.
(b) Projection of the allowed states onto the first Brillouin zone of graphene. Obviously, the K points are allowed states for CNTs of this chirality.
(c) 2-D illustration of the dispersion $W(k_x)$. The states at the Fermi level indicate the metallic behaviour of this tube. The periodicity volume in the k-space is given by the interval from -π/P to +π/P.

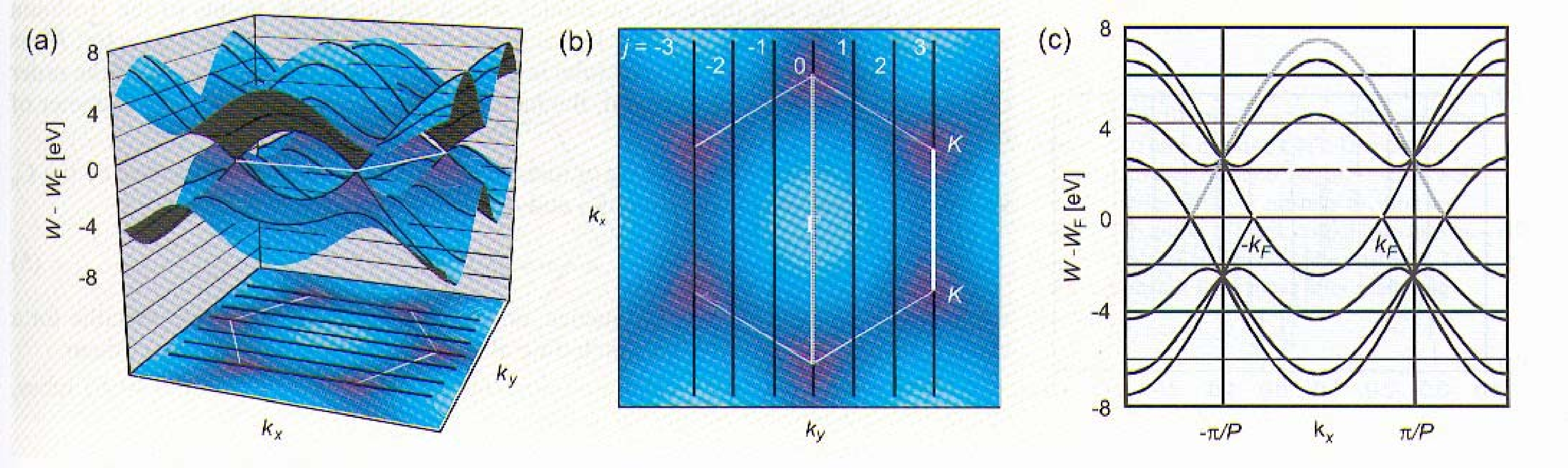

Electronic structure of CNT III

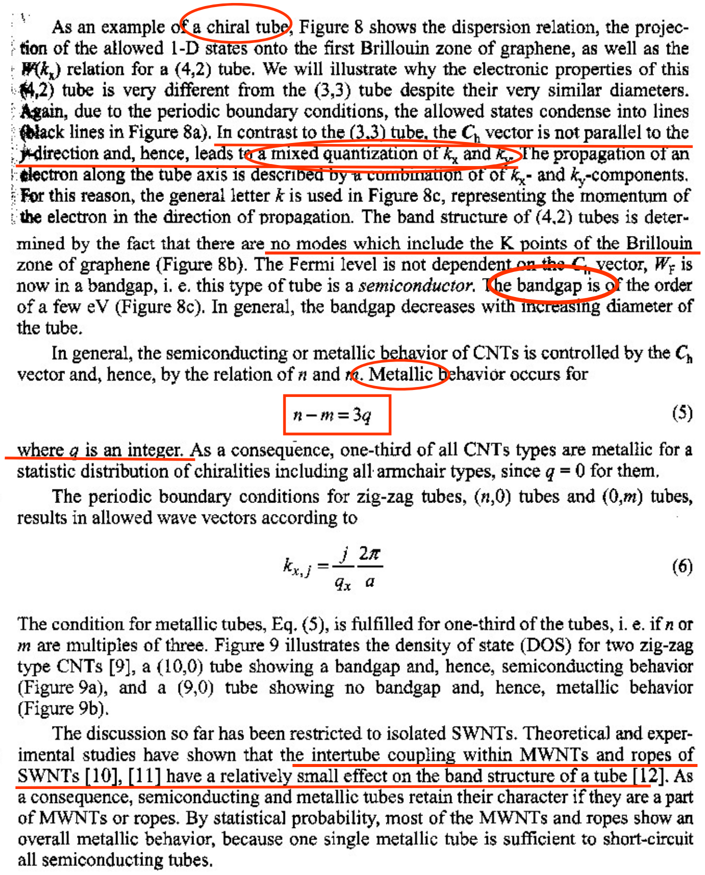

As an example of a chiral tube, Figure 8 shows the dispersion relation, the projection of the allowed 1-D states onto the first Brillouin zone of graphene, as well as the $W(k_x)$ relation for a (4,2) tube. We will illustrate why the electronic properties of this (4,2) tube is very different from the (3,3) tube despite their very similar diameters. Again, due to the periodic boundary conditions, the allowed states condense into lines (black lines in Figure 8a). In contrast to the (3,3) tube, the C_h vector is not parallel to the y-direction and, hence, leads to a mixed quantization of k_x and k_y. The propagation of an electron along the tube axis is described by a combination of of k_x- and k_y-components. For this reason, the general letter k is used in Figure 8c, representing the momentum of the electron in the direction of propagation. The band structure of (4,2) tubes is determined by the fact that there are no modes which include the K points of the Brillouin zone of graphene (Figure 8b). The Fermi level is not dependent on the C_h vector, W_F is now in a bandgap, i. e. this type of tube is a *semiconductor*. The bandgap is of the order of a few eV (Figure 8c). In general, the bandgap decreases with increasing diameter of the tube.

In general, the semiconducting or metallic behavior of CNTs is controlled by the C_h vector and, hence, by the relation of n and m. Metallic behavior occurs for

$$\boxed{n - m = 3q} \qquad (5)$$

where q is an integer. As a consequence, one-third of all CNTs types are metallic for a statistic distribution of chiralities including all armchair types, since $q = 0$ for them.

The periodic boundary conditions for zig-zag tubes, $(n,0)$ tubes and $(0,m)$ tubes, results in allowed wave vectors according to

$$k_{x,j} = \frac{j}{q_x} \frac{2\pi}{a} \qquad (6)$$

The condition for metallic tubes, Eq. (5), is fulfilled for one-third of the tubes, i. e. if n or m are multiples of three. Figure 9 illustrates the density of state (DOS) for two zig-zag type CNTs [9], a (10,0) tube showing a bandgap and, hence, semiconducting behavior (Figure 9a), and a (9,0) tube showing no bandgap and, hence, metallic behavior (Figure 9b).

The discussion so far has been restricted to isolated SWNTs. Theoretical and experimental studies have shown that the intertube coupling within MWNTs and ropes of SWNTs [10], [11] have a relatively small effect on the band structure of a tube [12]. As a consequence, semiconducting and metallic tubes retain their character if they are a part of MWNTs or ropes. By statistical probability, most of the MWNTs and ropes show an overall metallic behavior, because one single metallic tube is sufficient to short-circuit all semiconducting tubes.

Chiral CNT

Metal/semi

SWNT/MWNT

Periodic boundary conditions depend on the chirality

Electronic behavior depends on the structure:

- **armchair (n, n) are conductive**
- **n – m = 3q (q integer) are semi-metal**
- **otherwise, semiconductor**

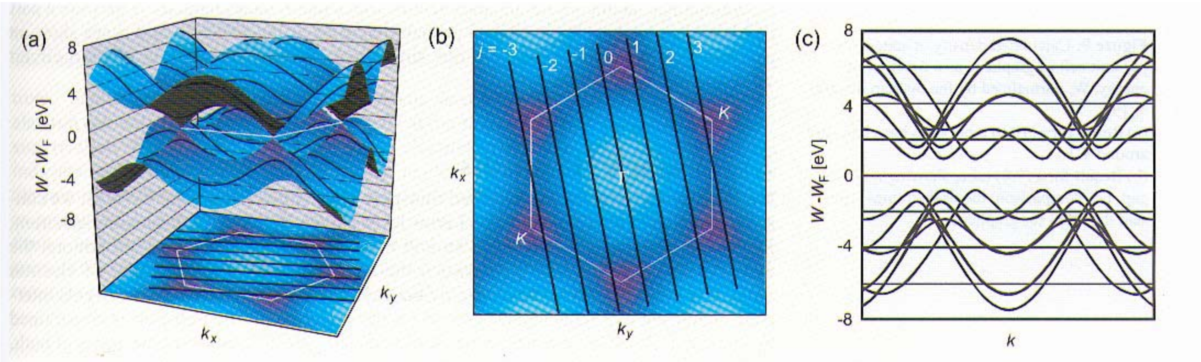

Figure 8: Dispersion relation of a (4,2) CNT.
(a) 3-D illustration of the dispersion relation for graphene including the allowed states for the (4,2) CNT. The periodic boundary conditions along the circumference of the tube result in a discrete set of allowed k values.
(b) Projection of the allowed states onto the first Brillouin zone of graphene. Obviously, the K points are no allowed states for CNTs of this chirality.
(c) 2-D illustration of the dispersion $W(k)$. the conduction band and the valence band are separated by a bandgap.

Resume of electronic properties in CNT

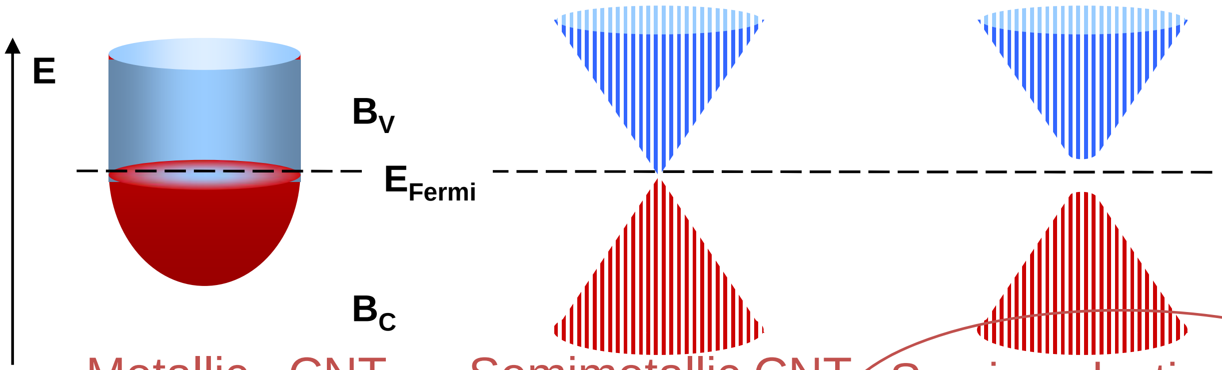

Metallic CNT

Armchair (n,n)

Semimetallic CNT

m-n=3q

Semiconducting CNT

m-n≠3q

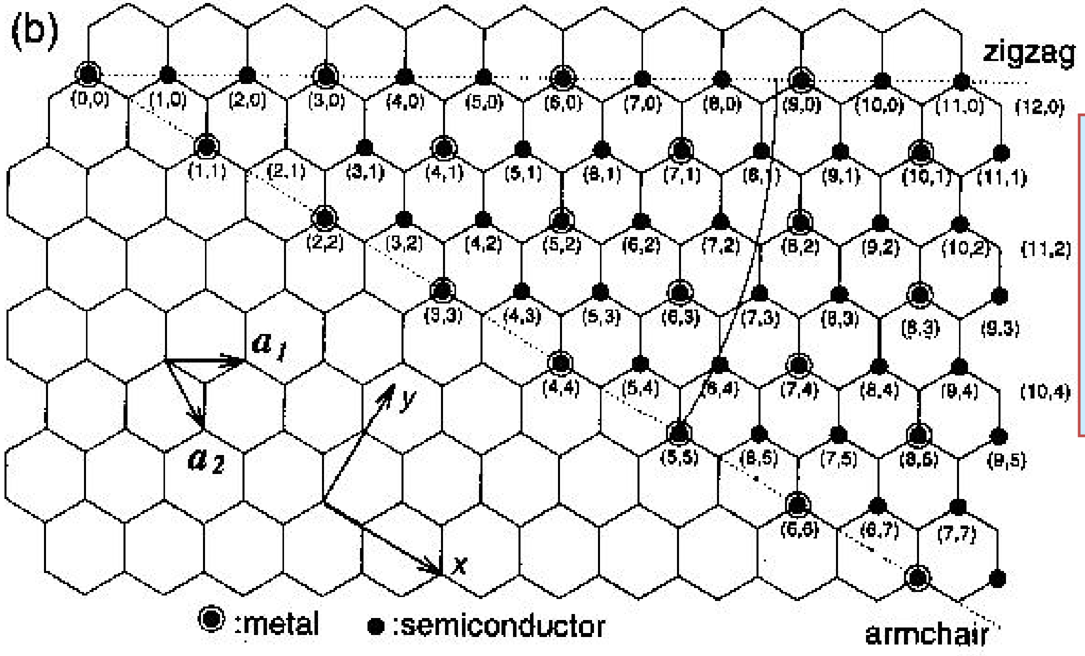

Tuneable band gap (2x10^{-3}-1.1eV)

E_g~1/d_{NT} also affected by:

chemical doping (B, N, O, Li, K, …)

point defects (e.g., pentagons, heptagons, instead of hexagons)

Some envisioned applications of CNT

Applications other than electronics:

- Hydrogen and ion (Li) storage units
- Supercapacitors, fuel cells, batteries
- Gas sensors
- FE devices **(field emitters)**
- Advanced scanning probes (SEM)
- Superstrong and tough composites **(nanocomposites)**
- Templates for metal nanowires
- Actuators **(NanoElectroMechanical Systems - NEMS)**
- …

Many applications exploit the unique mechanical properties and the 1D geometry of CNTs

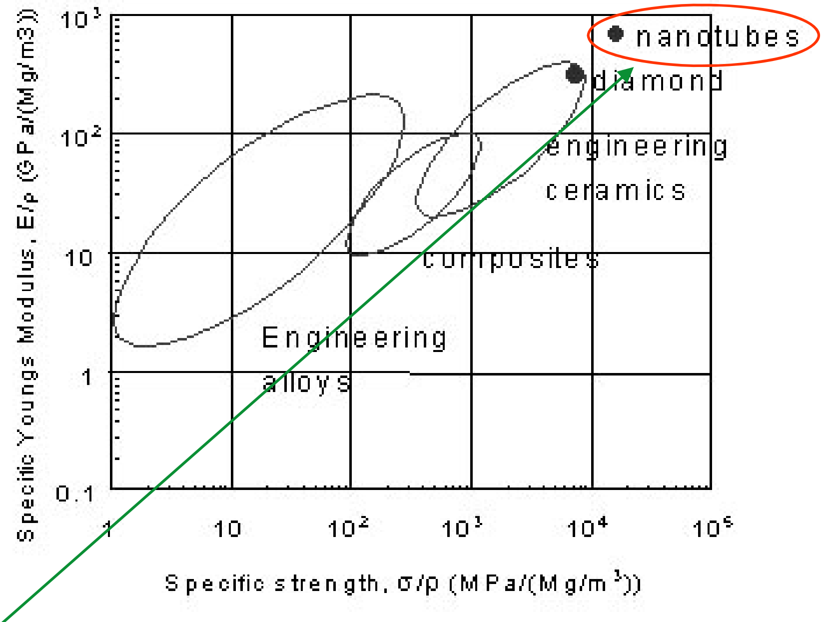

Comparison of Specific Young's Modulus vs. Specific Strength for nanotubes and other engineering materials

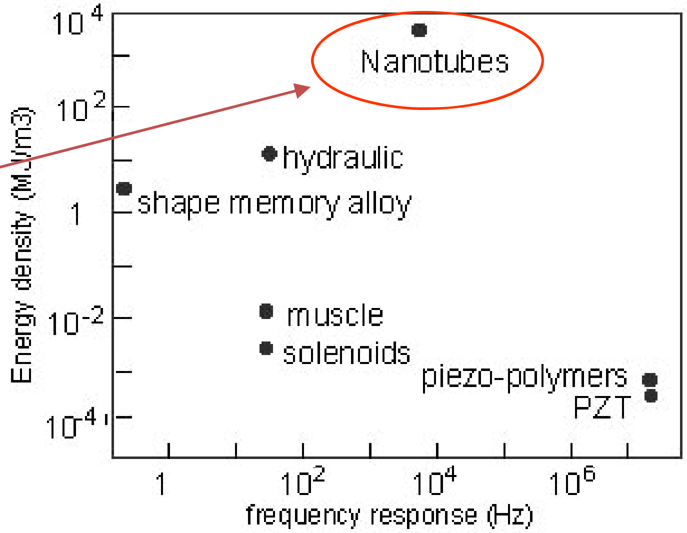

Fig. 3. Energy Density vs. Frequency response of Actuator materials

Mechanical properties of CNT I

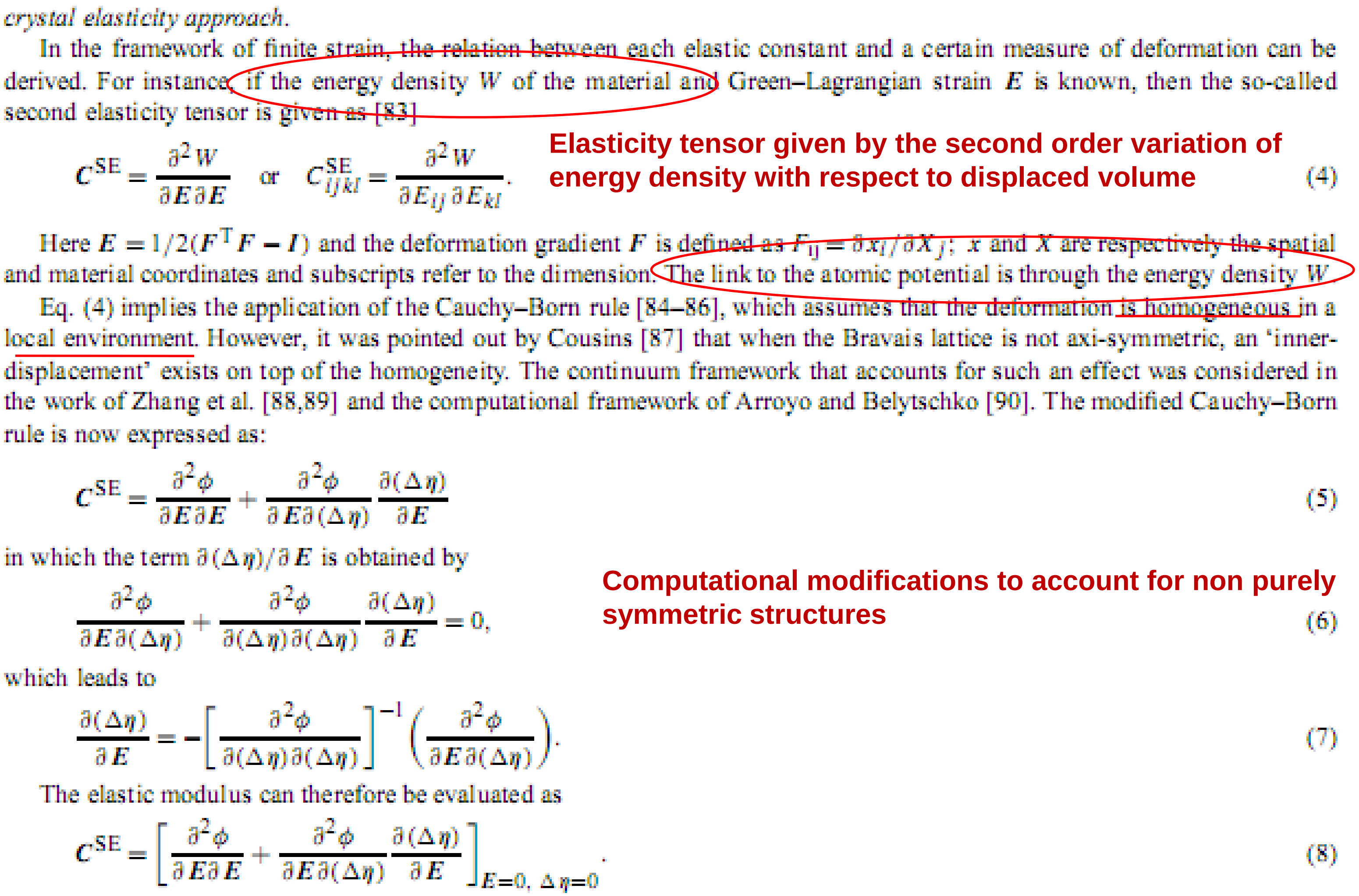

crystal elasticity approach.

In the framework of finite strain, the relation between each elastic constant and a certain measure of deformation can be derived. For instance, if the energy density W of the material and Green–Lagrangian strain $\boldsymbol{E}$ is known, then the so-called second elasticity tensor is given as [83]

$$C^{\mathrm{SE}} = \frac{\partial^2 W}{\partial \boldsymbol{E} \partial \boldsymbol{E}} \quad \text{or} \quad C^{\mathrm{SE}}_{ijkl} = \frac{\partial^2 W}{\partial E_{ij} \partial E_{kl}}. \tag{4}$$

Elasticity tensor given by the second order variation of energy density with respect to displaced volume

Here $\boldsymbol{E} = 1/2(\boldsymbol{F}^{\mathrm{T}}\boldsymbol{F} - \boldsymbol{I})$ and the deformation gradient $\boldsymbol{F}$ is defined as $F_{ij} = \partial x_i / \partial X_j$; x and X are respectively the spatial and material coordinates and subscripts refer to the dimension. The link to the atomic potential is through the energy density W.

Eq. (4) implies the application of the Cauchy–Born rule [84–86], which assumes that the deformation is homogeneous in a local environment. However, it was pointed out by Cousins [87] that when the Bravais lattice is not axi-symmetric, an 'inner-displacement' exists on top of the homogeneity. The continuum framework that accounts for such an effect was considered in the work of Zhang et al. [88,89] and the computational framework of Arroyo and Belytschko [90]. The modified Cauchy–Born rule is now expressed as:

$$C^{\mathrm{SE}} = \frac{\partial^2 \phi}{\partial \boldsymbol{E} \partial \boldsymbol{E}} + \frac{\partial^2 \phi}{\partial \boldsymbol{E} \partial (\Delta \eta)} \frac{\partial (\Delta \eta)}{\partial \boldsymbol{E}} \tag{5}$$

in which the term $\partial(\Delta\eta)/\partial \boldsymbol{E}$ is obtained by

$$\frac{\partial^2 \phi}{\partial \boldsymbol{E} \partial (\Delta \eta)} + \frac{\partial^2 \phi}{\partial (\Delta \eta) \partial (\Delta \eta)} \frac{\partial (\Delta \eta)}{\partial \boldsymbol{E}} = 0, \tag{6}$$

Computational modifications to account for non purely symmetric structures

which leads to

$$\frac{\partial (\Delta \eta)}{\partial \boldsymbol{E}} = -\left[\frac{\partial^2 \phi}{\partial (\Delta \eta) \partial (\Delta \eta)}\right]^{-1} \left(\frac{\partial^2 \phi}{\partial \boldsymbol{E} \partial (\Delta \eta)}\right). \tag{7}$$

The elastic modulus can therefore be evaluated as

$$C^{\mathrm{SE}} = \left[\frac{\partial^2 \phi}{\partial \boldsymbol{E} \partial \boldsymbol{E}} + \frac{\partial^2 \phi}{\partial \boldsymbol{E} \partial (\Delta \eta)} \frac{\partial (\Delta \eta)}{\partial \boldsymbol{E}}\right]_{\boldsymbol{E}=0,\ \Delta\eta=0}. \tag{8}$$

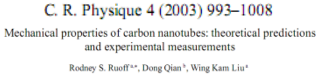

C. R. Physique 4 (2003) 993–1008

Mechanical properties of carbon nanotubes: theoretical predictions and experimental measurements

Rodney S. Ruoff, Dong Qian, Wing Kam Liu

Mechanical properties of CNT II

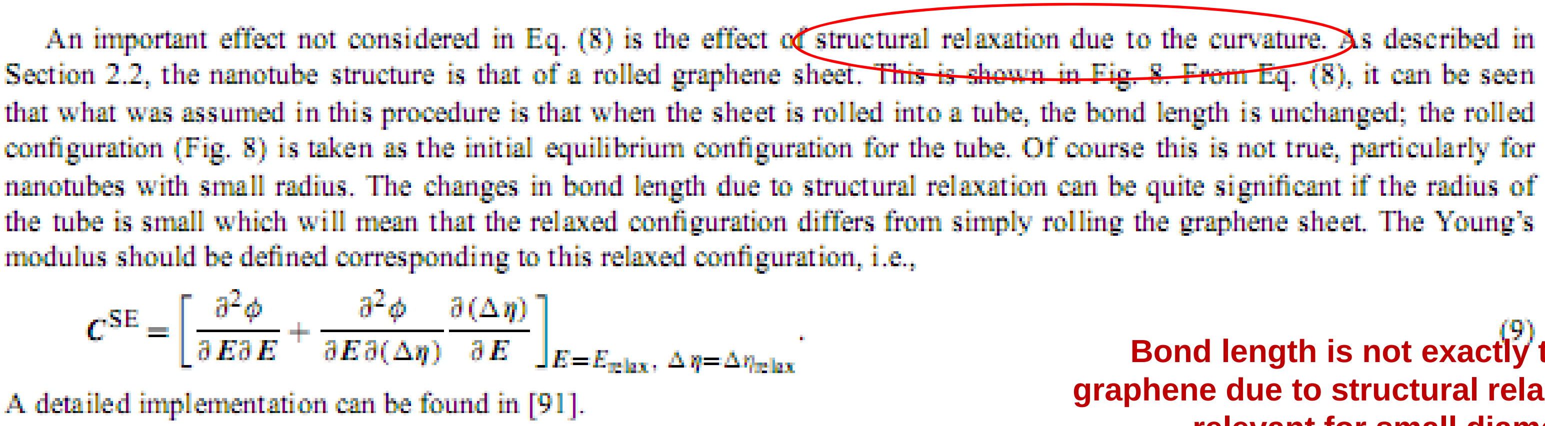

An important effect not considered in Eq. (8) is the effect of structural relaxation due to the curvature. As described in Section 2.2, the nanotube structure is that of a rolled graphene sheet. This is shown in Fig. 8. From Eq. (8), it can be seen that what was assumed in this procedure is that when the sheet is rolled into a tube, the bond length is unchanged; the rolled configuration (Fig. 8) is taken as the initial equilibrium configuration for the tube. Of course this is not true, particularly for nanotubes with small radius. The changes in bond length due to structural relaxation can be quite significant if the radius of the tube is small which will mean that the relaxed configuration differs from simply rolling the graphene sheet. The Young's modulus should be defined corresponding to this relaxed configuration, i.e.,

$$C^{\mathrm{SE}} = \left[\frac{\partial^2 \phi}{\partial E \partial E} + \frac{\partial^2 \phi}{\partial E \partial(\Delta\eta)} \frac{\partial(\Delta\eta)}{\partial E}\right]_{E=E_{\mathrm{relax}},\ \Delta\eta=\Delta\eta_{\mathrm{relax}}}. \tag{9}$$

A detailed implementation can be found in [91].

Bond length is not exactly the same as for graphene due to structural relaxation (particularly relevant for small diameter CNTs)!

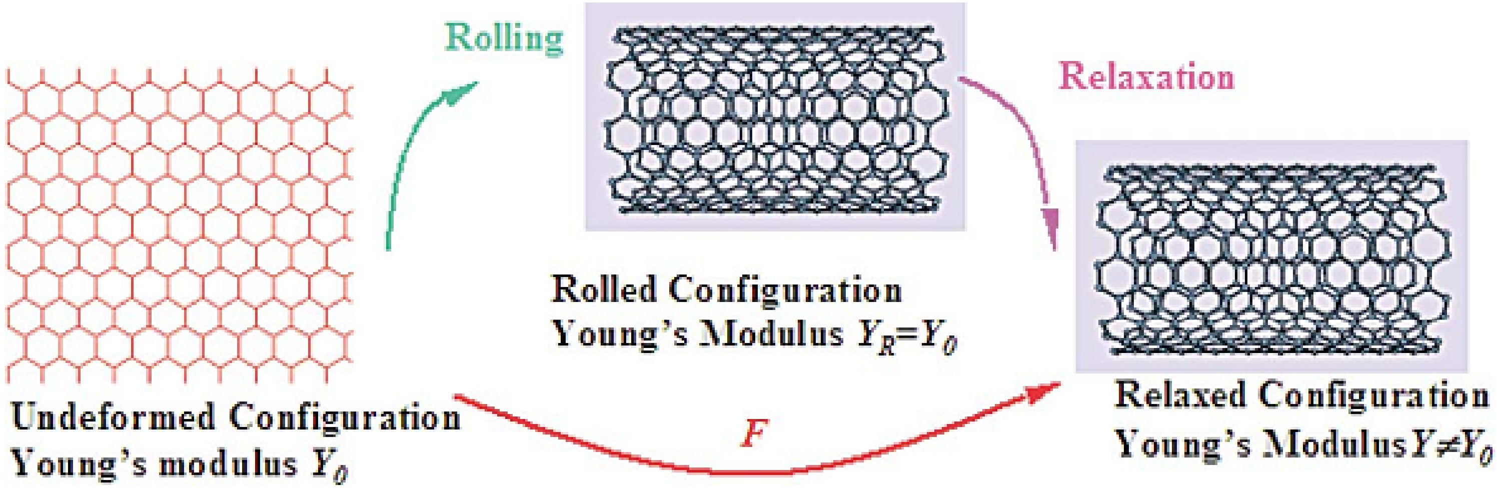

The cylindrical shape of CNT affects the energy density and its behavior as a function of displacement (volume change)

Mechanical properties of CNT III

1.1 Theoretical predictions

It is interesting to compare the different theoretical results concerning the Young's modulus and its dependence on the nanotube diameter and helicity. The results are found to vary with the type of method and the potentials used to describe the interatomic bonding. It is first instructive to use classical mechanics to identify the key points in the mechanics of CNTs. (We recommend the paper of Ruoff and Lorents as a good introduction to this problem. [6]) The Young's modulus can be written as the second derivative of the strain energy divided by the equilibrium volume. Continuum elastic theory predicts a $1/R^2$ variation of the strain energy, with an elastic constant equal to C_{11} of graphite (which corresponds to the Young's modulus parallel to the basal plane), independent of the tube diameter [7]. Therefore, in the classical approximation, the Young's modulus is not expected to vary when wrapping a graphene sheet into a cylinder. This is not surprising since the atomic structure is not taken into account, so the elastic constants are the same as in a planar geometry. We expect this classical approximation to be valid for large-diameter CNTs. The question now is, what happens in very small diameter tubes for which the atomic structure and bonding arrangement must be included in a realistic model. We have in hand a sufficiently large number of theoretical approaches [8–10] to answer that question at least qualitatively. Both ab initio and empirical potential-based methods have been used to calculate the strain energy as a function of the tube diameter (and helicity). They all agree that only small corrections to the $1/R^2$ behaviour are to be expected. As a consequence, only small deviations of the elastic constant along the axis (C_{33} in standard notation) are observed. It is worth noting that the dependence of the elastic constants on the nanotube diameter is found to be different for each model. For example, two different empirical potentials give different values for the elastic constant and show a different trend as a function of diameter. A decrease of C_{33} when the radius decreases is sometimes predicted, and in other cases the inverse behaviour is observed. We hope that high-precision experiments will give a definite answer to this dilemma. We agree with Cornwell and Wille that, "Simulations are not to be taken as a substitute for experiment, but rather can guide experiment, point out the most promising avenues to explore, and assist with interpretation".

Appl. Phys. A 69, 255–260 (1999) / Digital Object Identifier (DOI) 10.1007/s003399900114

Mechanical properties of carbon nanotubes

J.-P. Salvetat*, J.-M. Bonard, N.H. Thomson, A.J. Kulik, L. Forró, W. Benoit, L. Zuppiroli

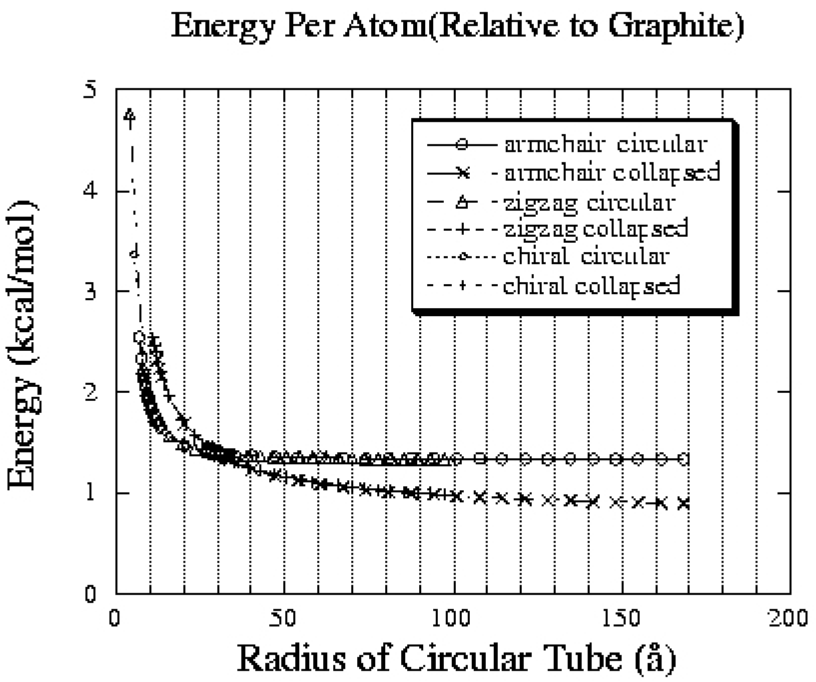

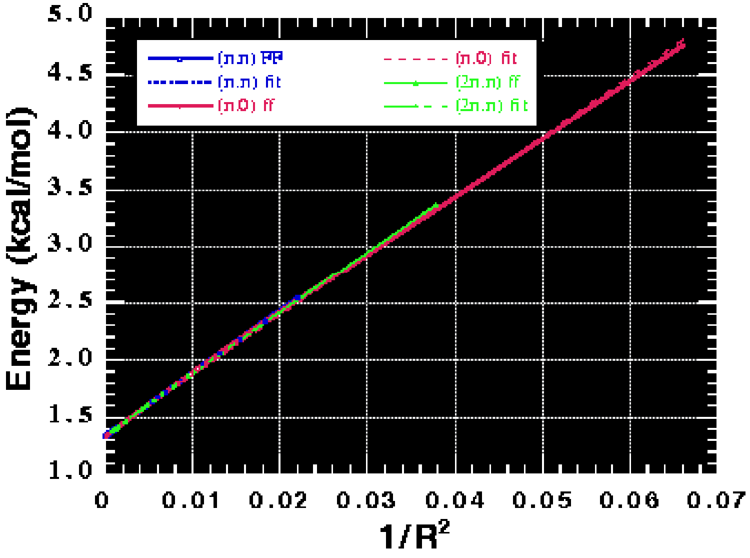

Figure 3: Strain energy as a function of tube radius

http://www.wag.c
l

Ductility/brittleness problems in CNT

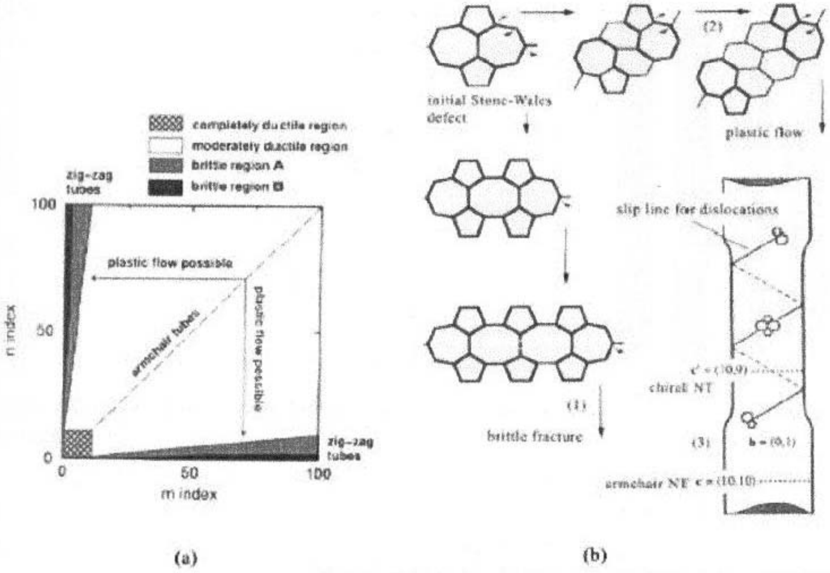

Figura 23 – (a) Mappa dei domini duttile/fragile per nanotubi di carbonio con diametri fino a 13 nm. Aree con diversa ombreggiatura corrispondono a differenti comportamenti del materiale; (b) Processo di propagazione di difetti in un nanotubo armchair con un iniziale difetto Stone-Wales. (1) frattura; (2) una coppia di dislocazioni scivolano via l'una dall'altra; (3) il cambio di chiralità del nanotubo e il graduale cambiamento del diametro causano una corrispondente variazione nelle proprietà elettriche. La formazione di ulteriori difetti Stone-Wales continua il processo di restringimento a meno che le dislocazioni non si impilino a causa della bassa temperatura che limita la mobilità sui tubi.

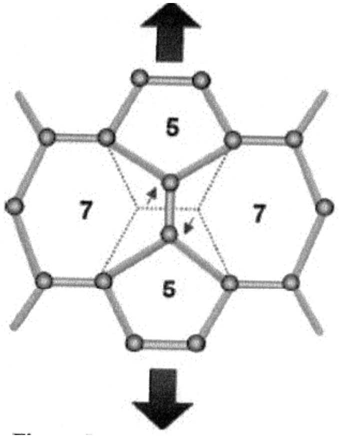

Stone Wales deformation

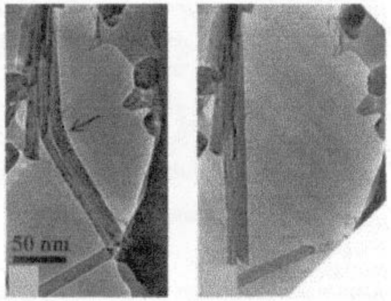

Figura 27 – Due immagini TEM mostrano un nanotubo (sx) originariamente piegato a temperatura ambiente e (dx.) dopo il riscaldamento

Heating up can restore the deformation

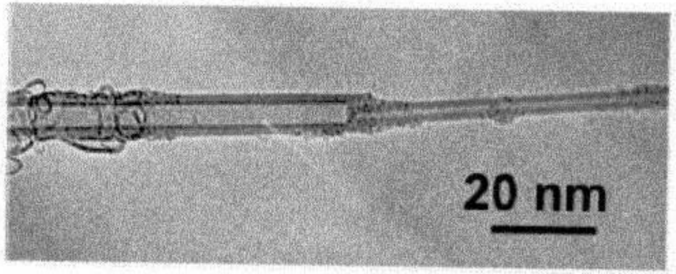

Figura 21 - Immagine TEM. Il nucleo interno a 4 strati è stato estratto (comportamento telescopico).

Telescopic behavior of MWNT under traction forces

Examples of NEMS with CNT I

Mechanical properties (and geometry) of CNTs make them excellent components of NanoElectroMechanical Systems (actuators, sensors, smart systems)

Science 21 May 1999:
Vol. 284. no. 5418, pp. 1340 - 1344
DOI: 10.1126/science.284.5418.1340

< Prev | Table of Contents | Ne

REPORTS

Carbon Nanotube Actuators

Ray H. Baughman, [1*] **Changxing Cui,** [1] **Anvar A. Zakhidov,** [1] **Zafar Iqbal,** [1] **Joseph N. Barisci,** [2] **Geoff M. Spinks,** [2] **Gordon G. Wallace,** [2] **Alberto Mazzoldi,** [3] **Danilo De Rossi,** [3] **Andrew G. Rinzler,** [4] **Oliver Jaschinski,** [5] **Siegmar Roth,** [5] **Miklos Kertesz** [6]

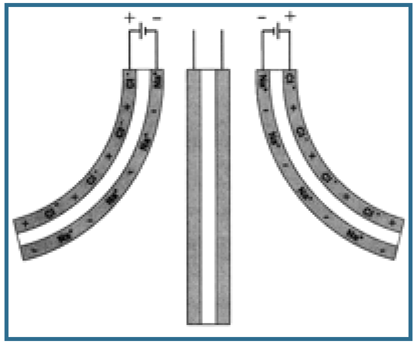

Fig. 3. Schematic edge-view of a cantilever-based actuator operated in aqueous NaCl, which consists of two strips of SWNTs (shaded) that are laminated together with an intermediate layer of double-sided Scotch tape (white). The Na^+ and Cl^- ions in the nanotube sheets represent ions in the double layer at the nanotube bundle surfaces, which are compensated by the indicated charges that are injected into the nanotube bundles. The equality between the lengths of the two nanotube sheets (center) is disrupted when a voltage is applied, causing the indicated actuator displacements to the left or right. The possible existence of a small amount of double-layer charge before the application of a voltage is ignored. [View Larger Version of this Image (40K GIF file)]

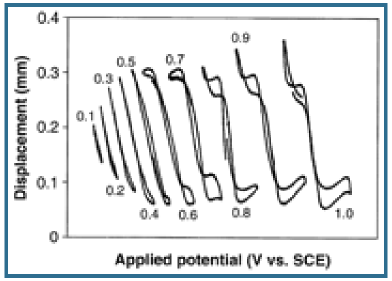

Fig. 5. Measured cantilever displacement (arbitrary origin) versus electrode potential (in 1 M NaCl) for a cantilever bimorph (Fig. 4A) in which two 15-µm-thick nanotube paper films bend a 215-µm-thick film of PVC. The potential range was symmetric about 0 V (versus a SCE), and the scan rate was 50 mV/s. The labels on the curves indicate the maximum applied potential. [View Larger Version of this Image (26K GIF file)]

Institute of Physics Publishing
Nanotechnology 16 (2005) 2548–2554 doi:10.1088/

Optically driven nanotube actuators

Shaoxin Lu and Balaji Panchapakesan

Optically driven actuators have been fabricated from single-wall carbon nanotube–polymer composite sheets. Like natural muscles, the millimetre-scale actuators are assemblies of millions of individual nanotube actuators processed into macroscopic length scales and bonded to an acrylic elastomer sheet to form an actuator that have been shown to generate higher stress than natural muscles and higher strains than high-modulus piezoelectric materials. Strain measurements revealed 0.01%–0.3% elastic strain generated due to electrostatic and thermal effects under visible light intensities of 5–120 mW cm^{-2}. An optically actuated nanotube gripper is demonstrated to show manipulation of small objects. This actuation technology overcomes some of the fundamental limitations such as the use of high voltages or electrochemical solutions for actuation, opening up possibilities for remote light-induced actuation technologies.

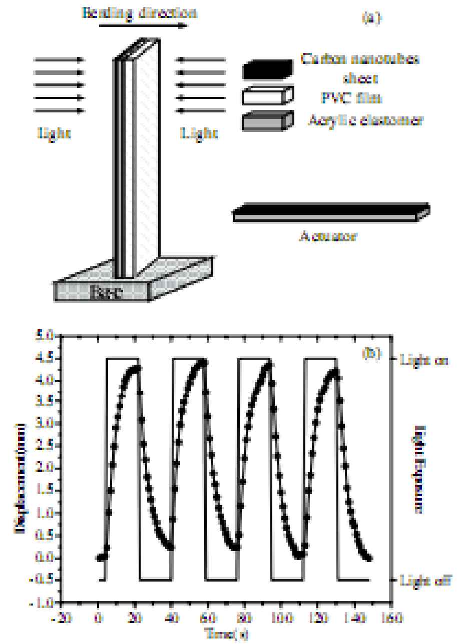

Figure 2. (a) A cantilever vertically anchored on a base. The cantilever is composed of an actuator (shown in the right lower part) and a 100 µm thick PVC film. (b) The displacement of the cantilever measured when light was turned on and off.

Examples of NEMS with CNT II

NATURE | VOL 424 | 24 JULY 2003 | www.nature.com/nature

Rotational actuators based on carbon nanotubes

A. M. Fennimore*, T. D. Yuzvinsky*, Wei-Qiang Han*, M. S. Fuhrer*†, J. Cumings*† & A. Zettl*

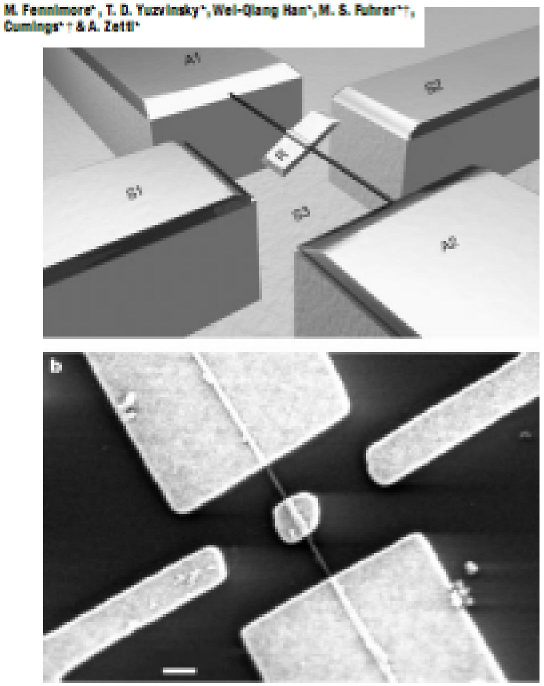

Figure 1 Integrated synthetic NEMS actuator. **a**, Conceptual drawing of nanoactuator. A metal plate rotor (R) is attached to a multi-walled carbon nanotube (MWNT) which acts as a a support shaft and is the source of rotational freedom. Electrical contact to the rotor plate is made via the MWNT and its anchor pads (A1, A2). Three stator electrodes, two on the SiO_2 surface (S1, S2) and one buried beneath the surface (S3), provide additional voltage control elements. The SiO_2 surface has been etched down to provide full rotational freedom for the rotor plate. The entire actuator assembly is integrated on a Si chip. **b**, Scanning electron microscope (SEM) image of nanoactuator just prior to HF etching. The actuator components can be identified by comparing this image to **a**. Scale bar, 300 nm.

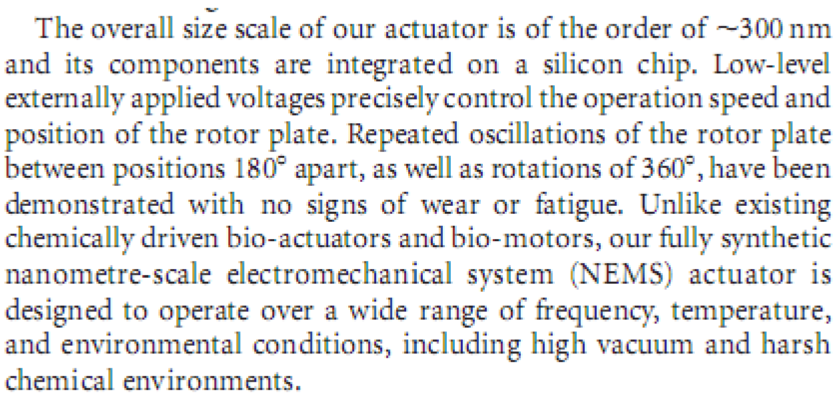

The overall size scale of our actuator is of the order of ~300 nm and its components are integrated on a silicon chip. Low-level externally applied voltages precisely control the operation speed and position of the rotor plate. Repeated oscillations of the rotor plate between positions 180° apart, as well as rotations of 360°, have been demonstrated with no signs of wear or fatigue. Unlike existing chemically driven bio-actuators and bio-motors, our fully synthetic nanometre-scale electromechanical system (NEMS) actuator is designed to operate over a wide range of frequency, temperature, and environmental conditions, including high vacuum and harsh chemical environments.

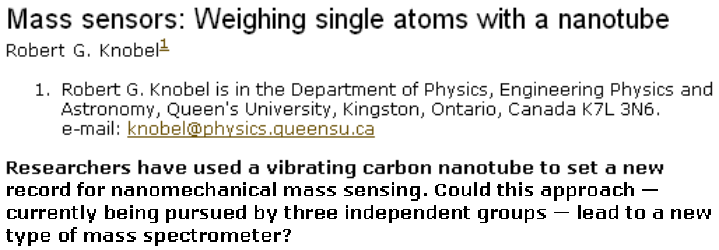

Mass sensors: Weighing single atoms with a nanotube

Robert G. Knobel[1]

1. Robert G. Knobel is in the Department of Physics, Engineering Physics and Astronomy, Queen's University, Kingston, Ontario, Canada K7L 3N6. e-mail: knobel@physics.queensu.ca

Researchers have used a vibrating carbon nanotube to set a new record for nanomechanical mass sensing. Could this approach — currently being pursued by three independent groups — lead to a new type of mass spectrometer?

Nanotube Tweezer

NanoLab offers two types of **Tweezers**--*three element nanotube tweezers* and *two element nanotube tweezers.*

Two element nanotube tweezer:

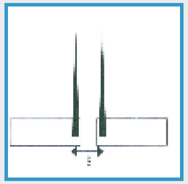

Substrate: 1x1cm oxide coated Si wafer
Contacts: two titanium electrode pads, 2x10 microns, separated by ~2 microns
Tweezer arms: On each electrode end, two carbon nanofibers (15 microns length x 100-200nm diameter) are deposited, with a separation distance (s) of 2 microns.
Pricing: $2530 ea
Operation: upon application of 8-12V DC, the tweezers will close. Limit current to 10 microamps.Tweezers typically remain closed upon removal of the voltage. To reopen, charge similarly, and bring a grounded probe near the closed end.
Customization: The nanofiber length, separation, and other geometric features can be customized on request. please contact our engineer Dan Esposito at danesposito@nano-lab.com

Mechanical properties of CNT composites

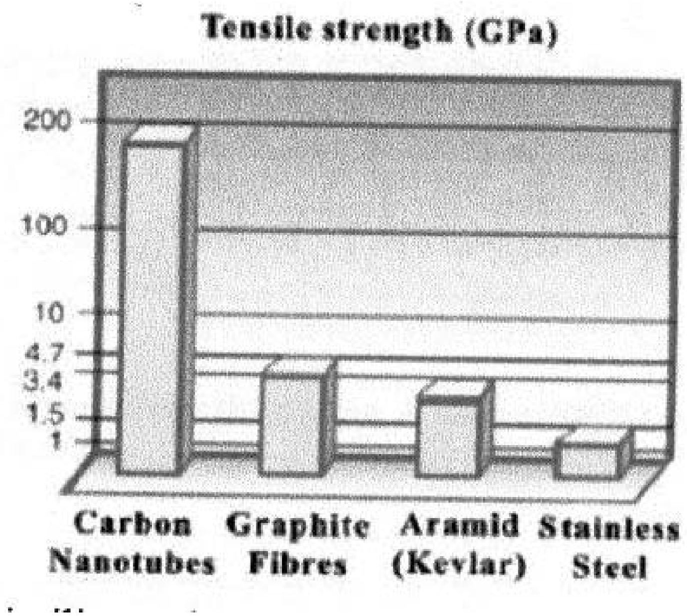

Young, shear and bulk modulus similar to diamond

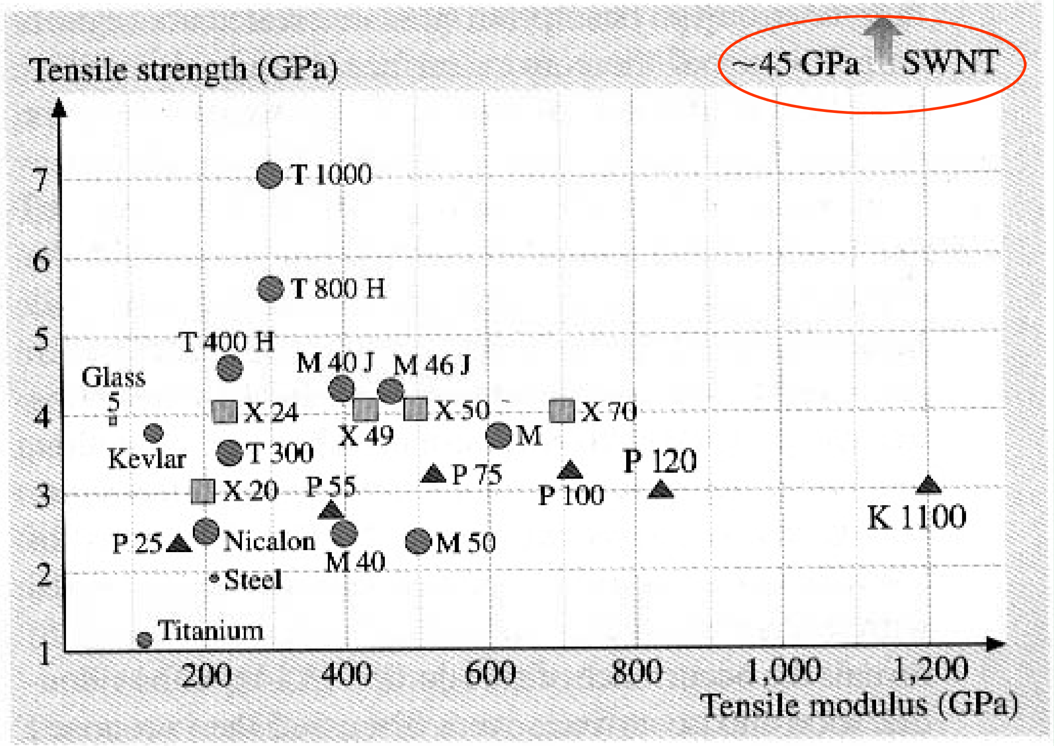

Fig. 3.23 Plot of the tensile strength versus tensile modulus for current fibrous materials, as compared to SWNTs. *Large circles* are PAN-based carbon fibers, which include the highest tensile strength fiber available on the market (T1000 from Torayca); *Triangles* are pitch-based carbon fibers, which include the highest tensile modulus fiber on the market (K1100 from Amoco)

Excellent mechanical properties due to strong intercarbon bonds and cylindrical geometry

⇩

Exploitations in structural materials

CNT-containing nanocomposites

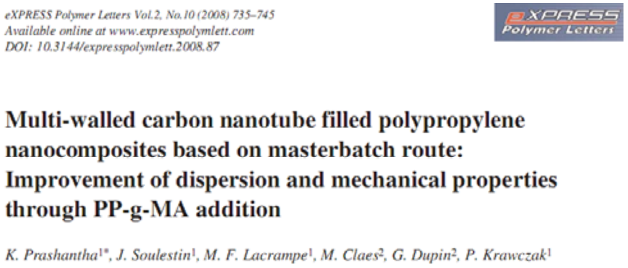
eXPRESS Polymer Letters Vol.2, No.10 (2008) 735–745
Available online at www.expresspolymlett.com
DOI: 10.3144/expresspolymlett.2008.87

Multi-walled carbon nanotube filled polypropylene nanocomposites based on masterbatch route: Improvement of dispersion and mechanical properties through PP-g-MA addition

K. Prashantha[1], J. Soulestin[1], M. F. Lacrampe[1], M. Claes[2], G. Dupin[2], P. Krawczak[1]*

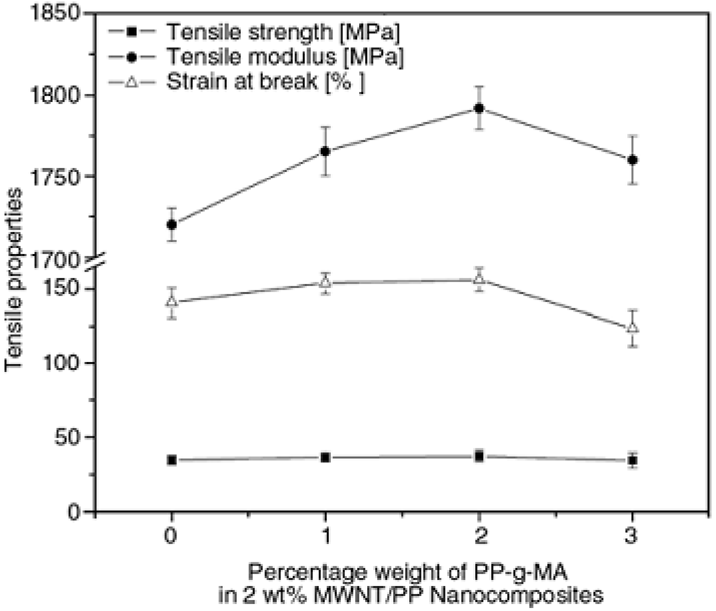

Figure 1. Effect of PP-g-MA content on tensile properties of PP/MWNT nanocomposites

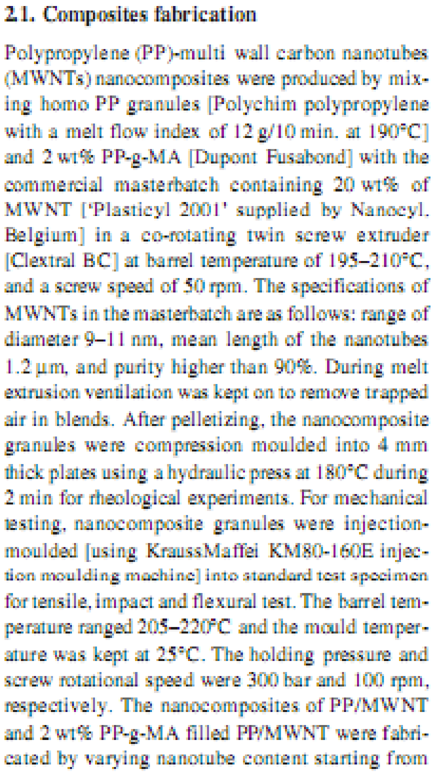
2.1. Composites fabrication

Polypropylene (PP)-multi wall carbon nanotubes (MWNTs) nanocomposites were produced by mixing homo PP granules [Polychim polypropylene with a melt flow index of 12 g/10 min. at 190°C] and 2 wt% PP-g-MA [Dupont Fusabond] with the commercial masterbatch containing 20 wt% of MWNT ['Plasticyl 2001' supplied by Nanocyl, Belgium] in a co-rotating twin screw extruder [Clextral BC] at barrel temperature of 195–210°C, and a screw speed of 50 rpm. The specifications of MWNTs in the masterbatch are as follows: range of diameter 9–11 nm, mean length of the nanotubes 1.2 µm, and purity higher than 90%. During melt extrusion ventilation was kept on to remove trapped air in blends. After pelletizing, the nanocomposite granules were compression moulded into 4 mm thick plates using a hydraulic press at 180°C during 2 min for rheological experiments. For mechanical testing, nanocomposite granules were injection-moulded [using KraussMaffei KM80-160E injection moulding machine] into standard test specimen for tensile, impact and flexural test. The barrel temperature ranged 205–220°C and the mould temperature was kept at 25°C. The holding pressure and screw rotational speed were 300 bar and 100 rpm, respectively. The nanocomposites of PP/MWNT and 2 wt% PP-g-MA filled PP/MWNT were fabricated by varying nanotube content starting from

Goal: to transfer the excellent mechanical properties of CNT to a composite material, including also a matrix (typical, polymer-based)

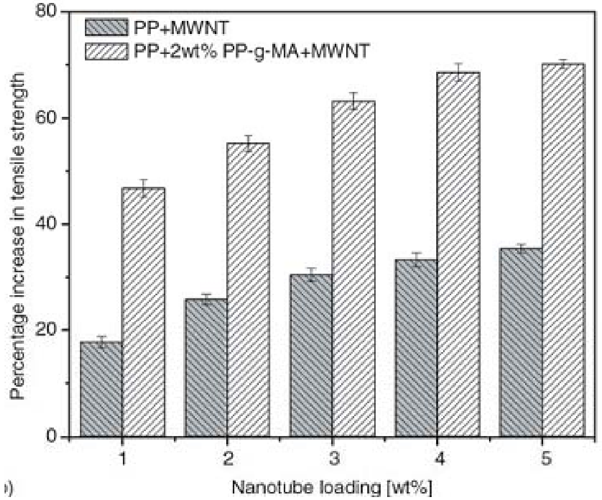

Multifunctional CNT nanocomposites

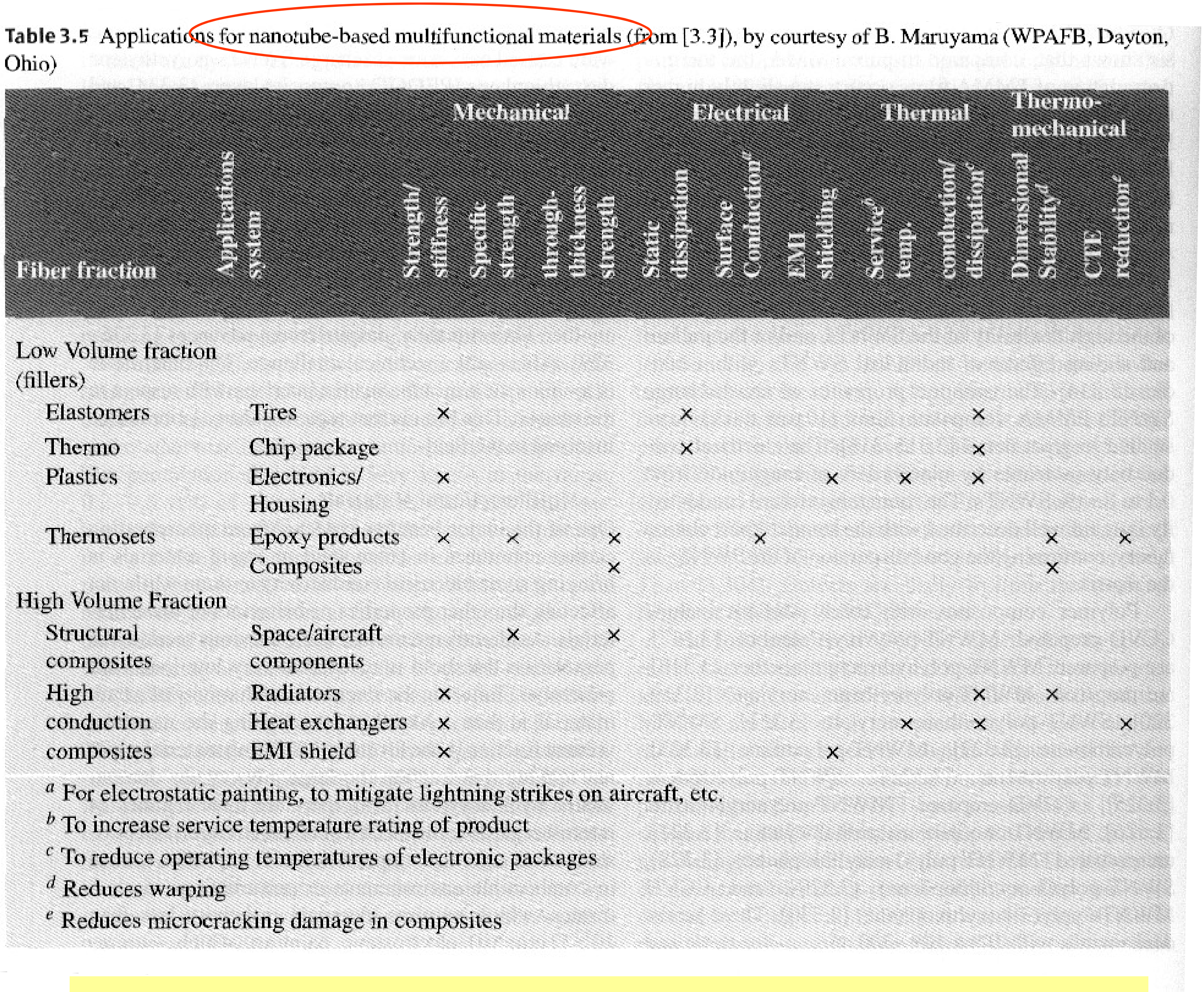

Table 3.5 Applications for nanotube-based multifunctional materials (from [3.3]), by courtesy of B. Maruyama (WPAFB, Dayton, Ohio)

Fiber fraction	Applications system	Mechanical			Electrical			Thermal		Thermo-mechanical	
		Strength/ stiffness	Specific strength	through-thickness strength	Static dissipation	Surface Conduction[a]	EMI shielding	Service[b] temp.	conduction/ dissipation[c]	Dimensional Stability[d]	CTE reduction[e]
Low Volume fraction (fillers)											
Elastomers	Tires	×			×				×		
Thermo Plastics	Chip package				×				×		
	Electronics/ Housing	×					×	×	×		
Thermosets	Epoxy products	×	×	×		×				×	×
	Composites			×						×	
High Volume Fraction											
Structural composites	Space/aircraft components		×	×							
High conduction composites	Radiators	×							×	×	
	Heat exchangers	×						×	×		×
	EMI shield	×					×				

[a] For electrostatic painting, to mitigate lightning strikes on aircraft, etc.

[b] To increase service temperature rating of product

[c] To reduce operating temperatures of electronic packages

[d] Reduces warping

[e] Reduces microcracking damage in composites

Wide variety of applications for CNT nanocomposites

Embedding CNT in a polymer matrix

Compatibility is an issue to avoid separation of CNT with respect to the matrix

CNT/polivinylalcohol

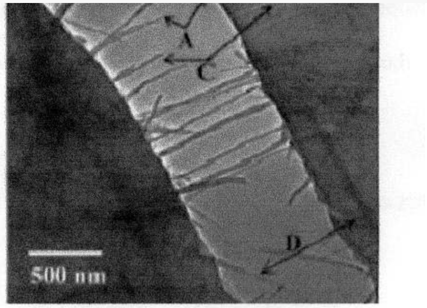

Figura 26 – Immagine SEM della superficie si frattura in un composito a base di nanotubi di carbonio.

Examples of functionalization

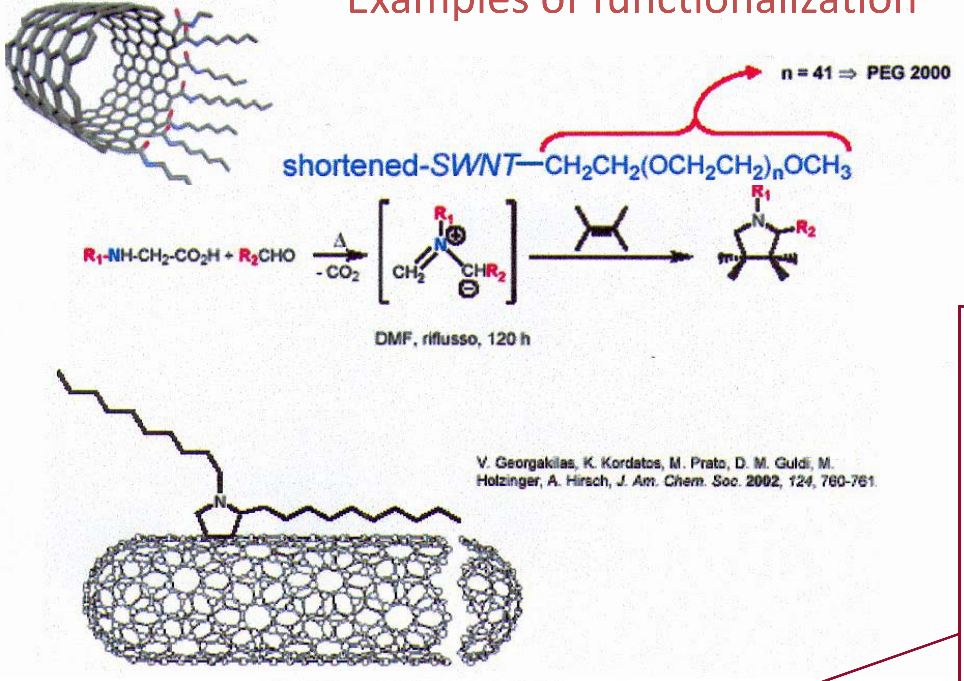

V. Georgakilas, K. Kordatos, M. Prato, D. M. Guldi, M. Holzinger, A. Hirsch, *J. Am. Chem. Soc.* **2002**, *124*, 760-761.

CNT funzionalizzato per solubilizzarlo in matrici polimeriche (es.: polietilenglicole attaccato a estremità di CNT “spezzati”, oppure AIBN - azobisiso butirronitrile che inizia legami covalenti tra carbonio e PMMA)

oppure surfattanti non-ionici per aumentare wettability

oppure miscelamenti meccanici prolungati (Brabender a doppia vite e temperatura alta)

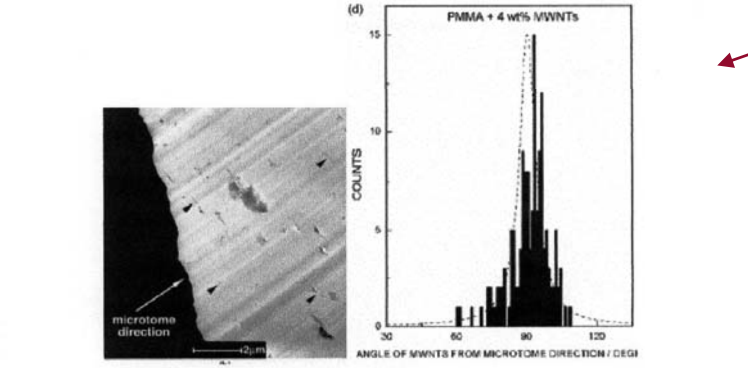

Figura 32 – (sx) Immagine TEM di un composito MWNT (4% in peso) in una matrice di PMMA. La freccia bianca indica la direzione del taglio (90° rispetto alla direzione di estrusione). Le frecce nere indicano i nanotubi. (dx) Istogramma che riporta la distribuzione di orientazione di MWCNT nel composito. La linea tratteggiata corrisponde a un fitting Lorentziano dei dati.

Other examples of CNT functionalization

Una prima reazione prevede la sospensione dei nanotubi in una soluzione 3:1 di acido solforico e nitrico in un bagno sonico per due ore, quindi per reazione con PDADMAC (polidiallildimetilammonio-Cloruro) che si aggancia ai gruppi carbossilici presenti in superficie, le particelle d'oro con diametro di 10 nm possono aderire:

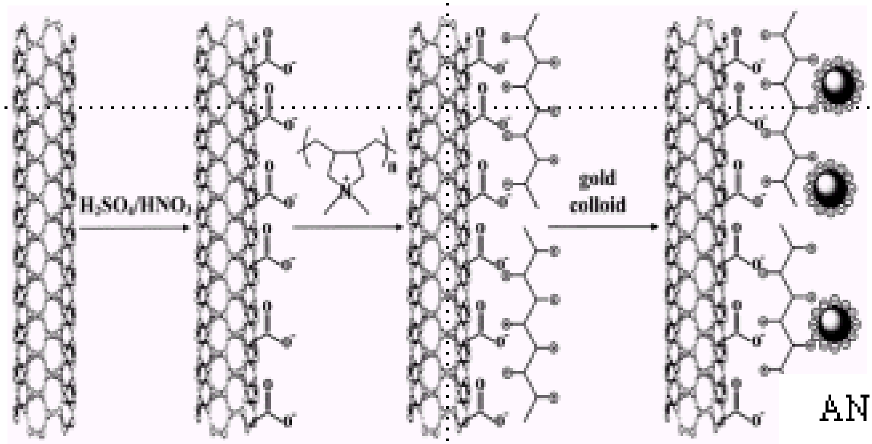

Gold nanoparticles can be grafted to the CNT wall through:

-Stabilization of nanoparticles by thiol (or ammine) groups

-An adhesion agent interposed between CNT wall and the nanoparticle

Further developments expected to lead to CNT functionalization by proteins or other biocompatibles

Materiale tratto dal seminario di M. Barnabò, Aprile 2004

Schematizzazione dell'attacco dei cluster di oro sulla superficie dei nanotubi:

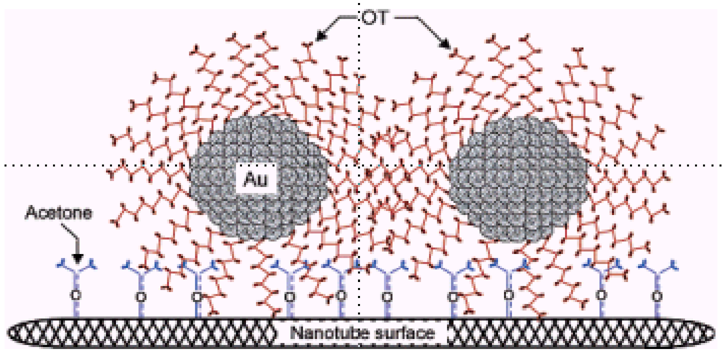

ANCORAGGIO DI NANOCLUSTER D'ORO SULLA SUPERFICIE DI NANOTUBI DI CARBONIO MODIFICATI

La modifica con acetone della superficie dei nanotubi di carbonio permette l'adesione di cluster metallici.
Nanoparticelle d'oro stabilizzate da opportuni leganti come tioli (o ammine) possono essere dunque adese su tali superfici dando luogo a strutture che potranno essere impiegate in nanodispositivi ibridi bio-inspired.
Infatti c'è un grande studio sulla possibilità di far aderire opportuni cluster stabilizzati da proteine su questi nanotubi quali parte di nanodispositivi
Per quanto riguarda il meccanismo di attacco esso è stato ipotizzato dai valori degli stretching asimmetrici dei CH_2 e CH_3 prima e dopo l'attacco dei cluster sui nanotubi e la conclusione è che si tratti di un'interazione tra le catene alchiliche dell'OT (ottandiolo) con i gruppi metilici dell'acetone.

Back to basics: the Nobel prize in physics, 2010 (yesterday)

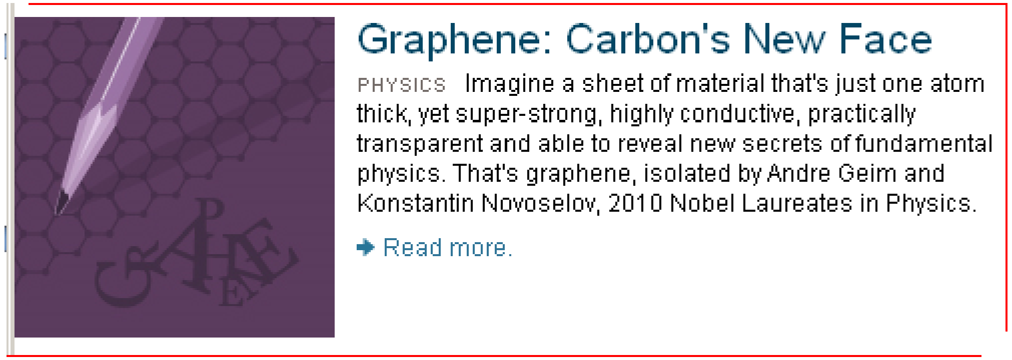

Graphene: Carbon's New Face

PHYSICS Imagine a sheet of material that's just one atom thick, yet super-strong, highly conductive, practically transparent and able to reveal new secrets of fundamental physics. That's graphene, isolated by Andre Geim and Konstantin Novoselov, 2010 Nobel Laureates in Physics.

➔ Read more.

Maybe, nanotube is too much in terms of structure to ensure exceptional provisions for new applications….

Photo: Sergeom, Wikimedia Commons

Andre Geim Konstantin Novoselov

The Nobel Prize in Physics 2010 was awarded jointly to Andre Geim and Konstantin Novoselov *"for groundbreaking experiments regarding the*

Small and ultra-small scales in mechanics: a resume

We have seen:

- The intimate (ultra-small sized) nature of materials involves quantum mechanics (e.g., phonons, specific heat,…)

- Mechanical interactions at the small scale can be modeled in the classical scenario (Lennard-Jones, van der Waals, Hertz), but they “include” quantum mechanics

- Small and ultra-small scale interactions can be:
  - ➢ Used to build novel microscopes (see AFM);
  - ➢ Measured to investigate materials and surfaces at the local scale

- Nanosized (isolated) structures may possess unique mechanical features, as ascertained in dedicated experiments: carbon nanotubes are an excellent example

- Atomic potential, a concept strictly related to ultra-small scale interactions, and its variation upon a mechanical perturbation are the main ingredients to understand the observed behavior

Intimate relationships exist between ultra-small, small and not small

We’ll mention now another (rather different) example

Mixing multiple length scales

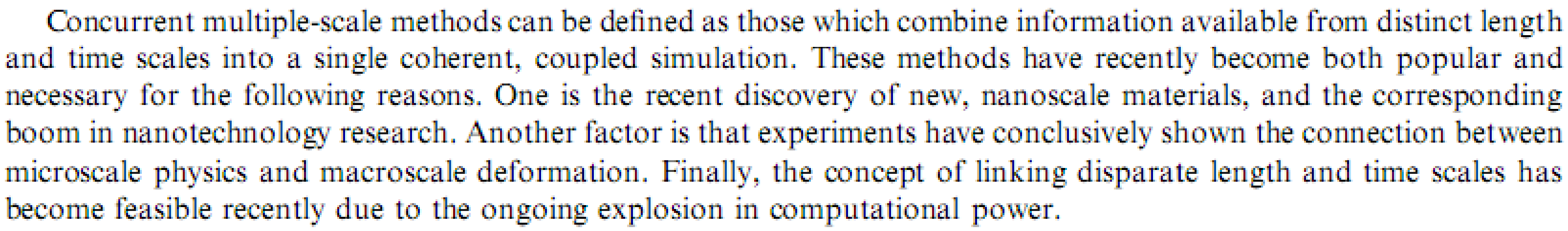

Concurrent multiple-scale methods can be defined as those which combine information available from distinct length and time scales into a single coherent, coupled simulation. These methods have recently become both popular and necessary for the following reasons. One is the recent discovery of new, nanoscale materials, and the corresponding boom in nanotechnology research. Another factor is that experiments have conclusively shown the connection between microscale physics and macroscale deformation. Finally, the concept of linking disparate length and time scales has become feasible recently due to the ongoing explosion in computational power.

Typical computational approaches:

- Finite Elements (FE) for macroscopic problems
- Molecular Dynamics (MD) for ultra-small scale problems

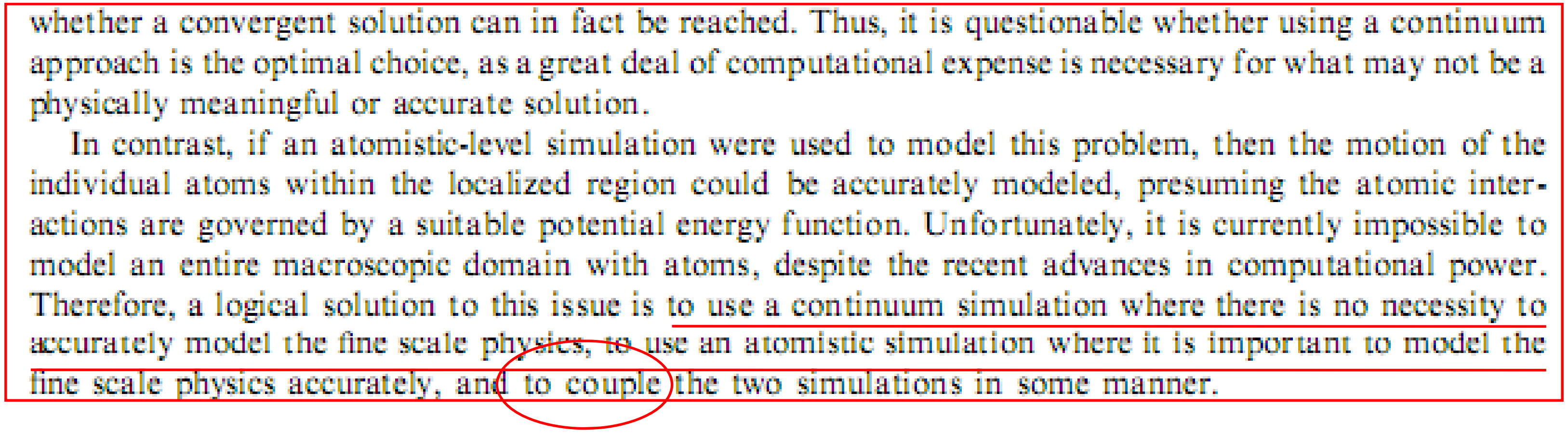

whether a convergent solution can in fact be reached. Thus, it is questionable whether using a continuum approach is the optimal choice, as a great deal of computational expense is necessary for what may not be a physically meaningful or accurate solution.

In contrast, if an atomistic-level simulation were used to model this problem, then the motion of the individual atoms within the localized region could be accurately modeled, presuming the atomic interactions are governed by a suitable potential energy function. Unfortunately, it is currently impossible to model an entire macroscopic domain with atoms, despite the recent advances in computational power. Therefore, a logical solution to this issue is to use a continuum simulation where there is no necessity to accurately model the fine scale physics, to use an atomistic simulation where it is important to model the fine scale physics accurately, and to couple the two simulations in some manner.

Comput. Methods Appl. Mech. Engrg. 193 (2004) 1733–1772

An introduction and tutorial on multiple-scale analysis
in solids

Harold S. Park *, Wing Kam Liu

Where to put the ultra-small scale

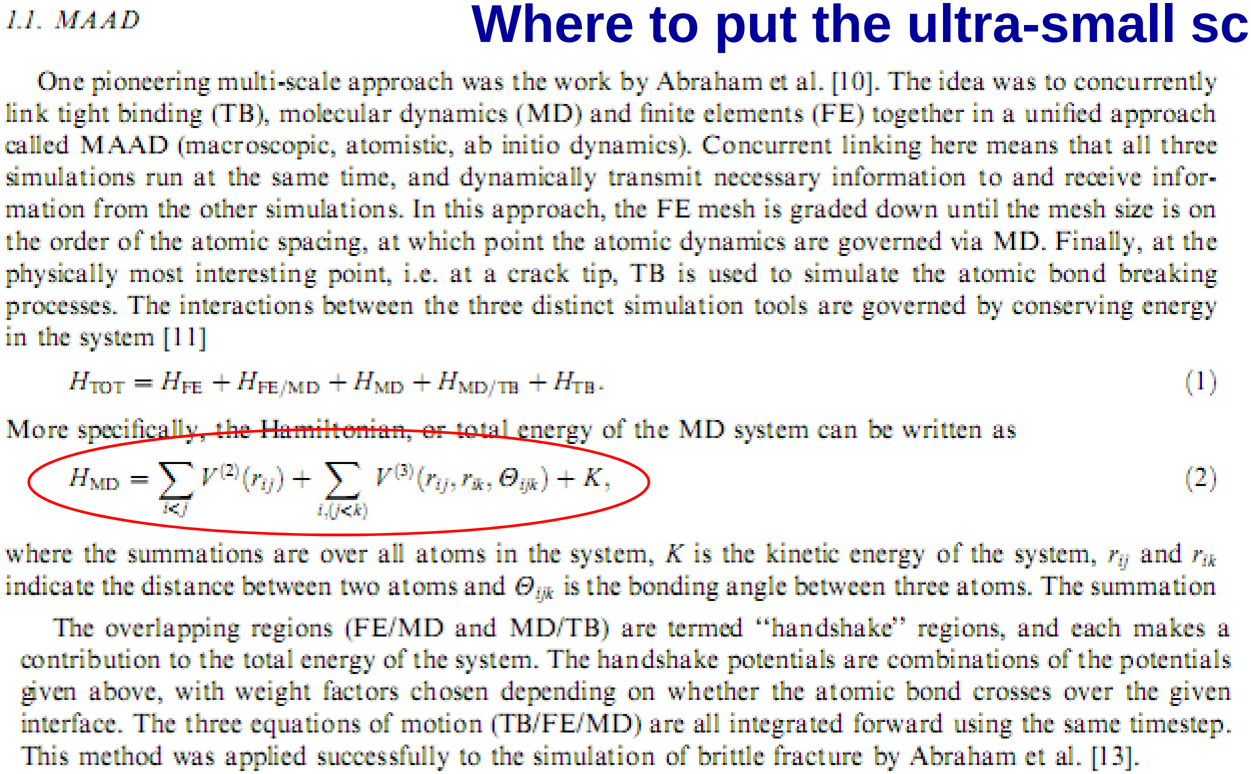

1.1. MAAD

One pioneering multi-scale approach was the work by Abraham et al. [10]. The idea was to concurrently link tight binding (TB), molecular dynamics (MD) and finite elements (FE) together in a unified approach called MAAD (macroscopic, atomistic, ab initio dynamics). Concurrent linking here means that all three simulations run at the same time, and dynamically transmit necessary information to and receive information from the other simulations. In this approach, the FE mesh is graded down until the mesh size is on the order of the atomic spacing, at which point the atomic dynamics are governed via MD. Finally, at the physically most interesting point, i.e. at a crack tip, TB is used to simulate the atomic bond breaking processes. The interactions between the three distinct simulation tools are governed by conserving energy in the system [11]

$$H_{\mathrm{TOT}} = H_{\mathrm{FE}} + H_{\mathrm{FE/MD}} + H_{\mathrm{MD}} + H_{\mathrm{MD/TB}} + H_{\mathrm{TB}}. \tag{1}$$

More specifically, the Hamiltonian, or total energy of the MD system can be written as

$$H_{\mathrm{MD}} = \sum_{i<j} V^{(2)}(r_{ij}) + \sum_{i,(j<k)} V^{(3)}(r_{ij}, r_{ik}, \Theta_{ijk}) + K, \tag{2}$$

where the summations are over all atoms in the system, K is the kinetic energy of the system, r_{ij} and r_{ik} indicate the distance between two atoms and Θ_{ijk} is the bonding angle between three atoms. The summation

The overlapping regions (FE/MD and MD/TB) are termed "handshake" regions, and each makes a contribution to the total energy of the system. The handshake potentials are combinations of the potentials given above, with weight factors chosen depending on whether the atomic bond crosses over the given interface. The three equations of motion (TB/FE/MD) are all integrated forward using the same timestep. This method was applied successfully to the simulation of brittle fracture by Abraham et al. [13].

FE
MD
(TB – for considering the locally deformed bonds)

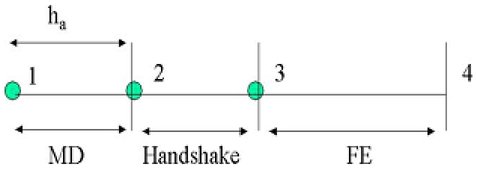

Fig. 5. Problem description for 1D MD/FE coupling.

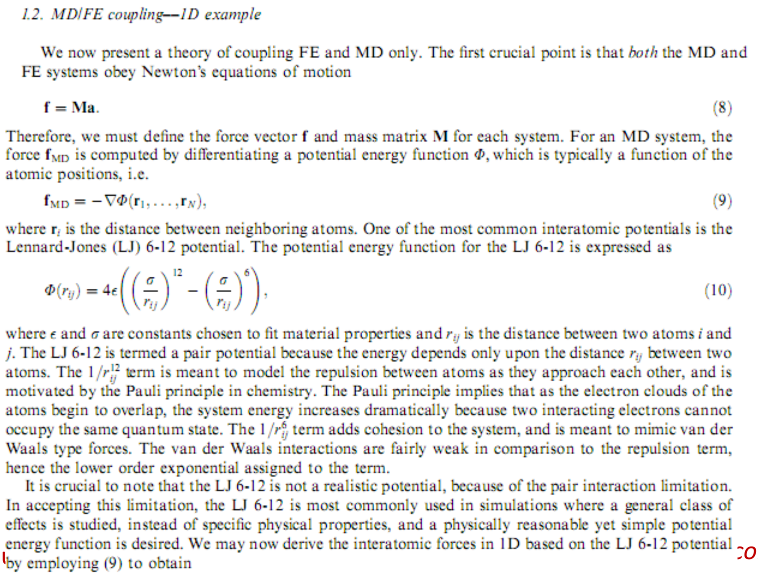

1.2. MD/FE coupling—1D example

We now present a theory of coupling FE and MD only. The first crucial point is that *both* the MD and FE systems obey Newton's equations of motion

$$\mathbf{f} = \mathbf{M}\mathbf{a}. \tag{8}$$

Therefore, we must define the force vector $\mathbf{f}$ and mass matrix $\mathbf{M}$ for each system. For an MD system, the force $\mathbf{f}_{\mathrm{MD}}$ is computed by differentiating a potential energy function Φ, which is typically a function of the atomic positions, i.e.

$$\mathbf{f}_{\mathrm{MD}} = -\nabla\Phi(\mathbf{r}_1, \ldots, \mathbf{r}_N), \tag{9}$$

where $\mathbf{r}_i$ is the distance between neighboring atoms. One of the most common interatomic potentials is the Lennard-Jones (LJ) 6-12 potential. The potential energy function for the LJ 6-12 is expressed as

$$\Phi(r_{ij}) = 4\epsilon\left(\left(\frac{\sigma}{r_{ij}}\right)^{12} - \left(\frac{\sigma}{r_{ij}}\right)^{6}\right), \tag{10}$$

where ϵ and σ are constants chosen to fit material properties and r_{ij} is the distance between two atoms i and j. The LJ 6-12 is termed a pair potential because the energy depends only upon the distance r_{ij} between two atoms. The $1/r_{ij}^{12}$ term is meant to model the repulsion between atoms as they approach each other, and is motivated by the Pauli principle in chemistry. The Pauli principle implies that as the electron clouds of the atoms begin to overlap, the system energy increases dramatically because two interacting electrons cannot occupy the same quantum state. The $1/r_{ij}^{6}$ term adds cohesion to the system, and is meant to mimic van der Waals type forces. The van der Waals interactions are fairly weak in comparison to the repulsion term, hence the lower order exponential assigned to the term.

It is crucial to note that the LJ 6-12 is not a realistic potential, because of the pair interaction limitation. In accepting this limitation, the LJ 6-12 is most commonly used in simulations where a general class of effects is studied, instead of specific physical properties, and a physically reasonable yet simple potential energy function is desired. We may now derive the interatomic forces in 1D based on the LJ 6-12 potential by employing (9) to obtain

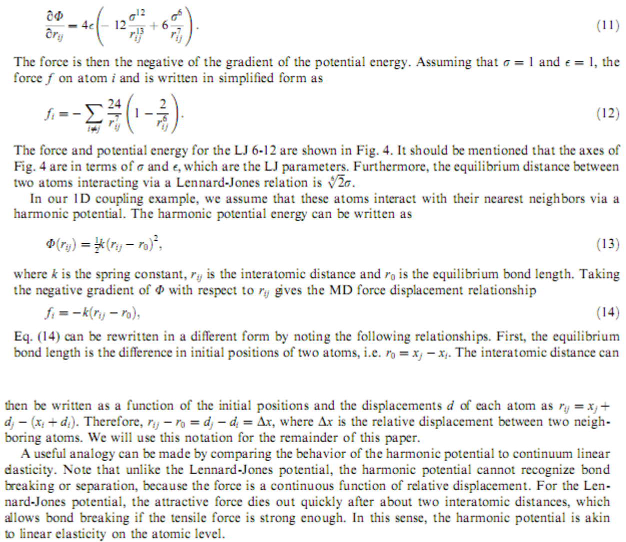

$$\frac{\partial\Phi}{\partial r_{ij}} = 4\epsilon\left(-12\frac{\sigma^{12}}{r_{ij}^{13}} + 6\frac{\sigma^{6}}{r_{ij}^{7}}\right). \tag{11}$$

The force is then the negative of the gradient of the potential energy. Assuming that $\sigma = 1$ and $\epsilon = 1$, the force f on atom i and is written in simplified form as

$$f_i = -\sum_{i \neq j} \frac{24}{r_{ij}^{7}}\left(1 - \frac{2}{r_{ij}^{6}}\right). \tag{12}$$

The force and potential energy for the LJ 6-12 are shown in Fig. 4. It should be mentioned that the axes of Fig. 4 are in terms of σ and ϵ, which are the LJ parameters. Furthermore, the equilibrium distance between two atoms interacting via a Lennard-Jones relation is $\sqrt[6]{2}\sigma$.

In our 1D coupling example, we assume that these atoms interact with their nearest neighbors via a harmonic potential. The harmonic potential energy can be written as

$$\Phi(r_{ij}) = \tfrac{1}{2}k(r_{ij} - r_0)^2, \tag{13}$$

where k is the spring constant, r_{ij} is the interatomic distance and r_0 is the equilibrium bond length. Taking the negative gradient of Φ with respect to r_{ij} gives the MD force displacement relationship

$$f_i = -k(r_{ij} - r_0), \tag{14}$$

Eq. (14) can be rewritten in a different form by noting the following relationships. First, the equilibrium bond length is the difference in initial positions of two atoms, i.e. $r_0 = x_j - x_i$. The interatomic distance can

then be written as a function of the initial positions and the displacements d of each atom as $r_{ij} = x_j + d_j - (x_i + d_i)$. Therefore, $r_{ij} - r_0 = d_j - d_i = \Delta x$, where Δx is the relative displacement between two neighboring atoms. We will use this notation for the remainder of this paper.

A useful analogy can be made by comparing the behavior of the harmonic potential to continuum linear elasticity. Note that unlike the Lennard-Jones potential, the harmonic potential cannot recognize bond breaking or separation, because the force is a continuous function of relative displacement. For the Lennard-Jones potential, the attractive force dies out quickly after about two interatomic distances, which allows bond breaking if the tensile force is strong enough. In this sense, the harmonic potential is akin to linear elasticity on the atomic level.

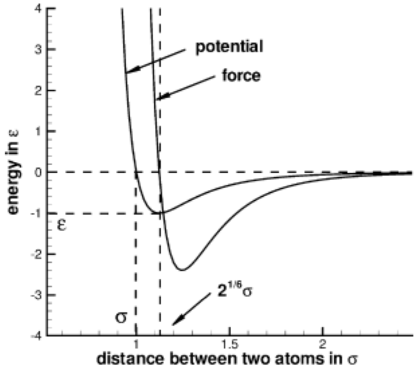

Fig. 4. Force and potential energy plot for Lennard-Jones 6-12 potential.

Example of multi-scale simulation

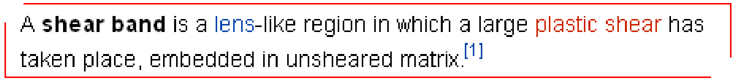

A **shear band** is a lens-like region in which a large plastic shear has taken place, embedded in unsheared matrix.[1]

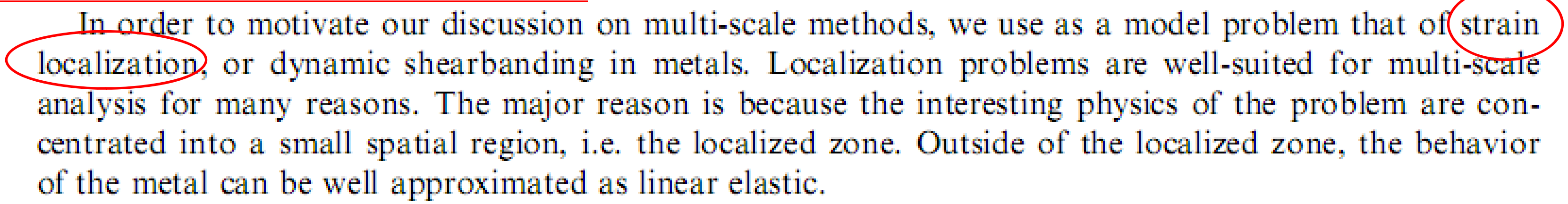

In order to motivate our discussion on multi-scale methods, we use as a model problem that of strain localization, or dynamic shearbanding in metals. Localization problems are well-suited for multi-scale analysis for many reasons. The major reason is because the interesting physics of the problem are concentrated into a small spatial region, i.e. the localized zone. Outside of the localized zone, the behavior of the metal can be well approximated as linear elastic.

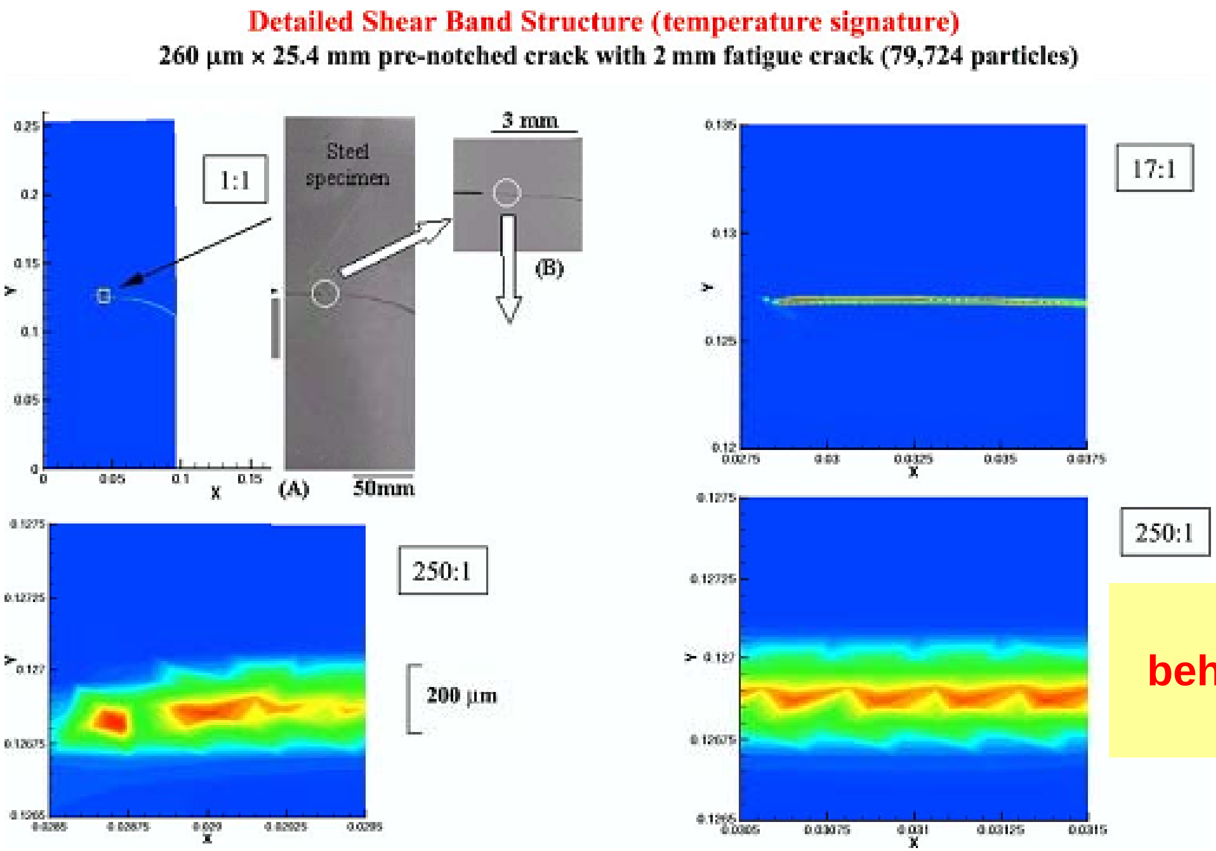

Detailed Shear Band Structure (temperature signature)

260 µm × 25.4 mm pre-notched crack with 2 mm fatigue crack (79,724 particles)

Fig. 1. Comparison of experimental and numerical results. From [3].

Local/macroscopic behaviors coupled together (and duly described)

Integrating defects in the description

polycrystalline solid - contains several crystalline regions which are randomly oriented

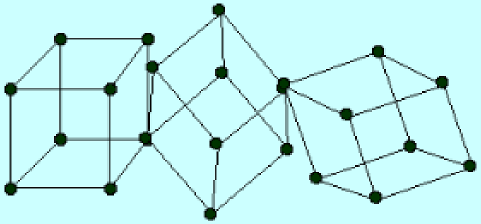

Most crystalline materials have many defects.

Some (like Silicon) can be grown with relatively few defects.

1. Planar defects - grain boundaries

interfaces between two single crystal regions of different orientation

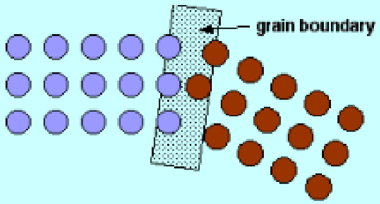

atoms at grain boundaries tend to be loosely bound

=> more reactive (corrosion) and accelerated diffusion along grain boundaries

typical grain sizes: 0.01 mm - 100 mm (micron)

2. line defects - dislocations

example: edge dislocation - from inserting an extra row of atoms

distorts lattice => stresses (compression and tension)

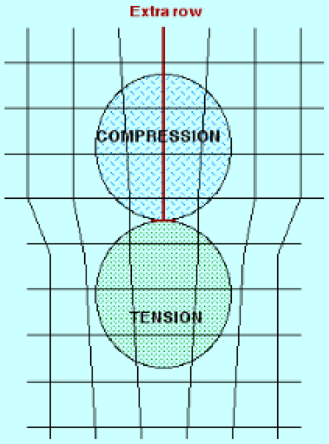

very common: often 10^{10} - 10^{12} dislocations/ cm^2 in films

3. point defects

- self interstitial - extra atom
- vacancy - missing atom
- substitutional impurity - impurity atom in lattice
- interstitial impurity - impurity atom not in regular lattice site

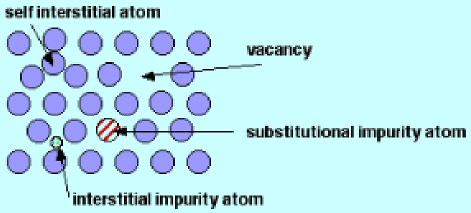

in principle you can eliminate all of these except vacancies

vacancies arise from thermodynamics (entropy)

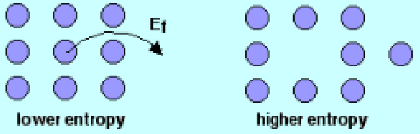

fraction of vacancies (f)

$$f = e^{-E_f / k_B T}$$

where k_B = Boltzmann's constant = 1.381 x 10^{-23} J/K

typically E_f is about 1 eV

at room temperature, f is about 10^{-17}

Goal: to improve description (and predictions) considering local defects (at the ultra-small scale)

http://www.uccs.edu/~tchriste/courses/PHYS549/549lectures/defects.html

Conclusions

- ✓ Small scale structures, e.g., nanostructures, can exhibit unique properties

- ✓ The example of carbon nanotubes is highly suited:
  - o CNT can be easily produced;
  - o CNT are stable and own excellent Young modulus;
  - o CNT can be tuned, at least in principle, for electronic properties

- ✓ In isolated nanostructures the ultra-small (atomistic) properties determine the main features of the system

- ✓ Such an interplay can be seen also in a completely different area, dealing with fracture and localized stress phenomena and with their simulation

- ✓ But: mechanics is not everything, and it’s now time to move to other properties (optical, electronics)